Joint Duplex Mode Selection and Beamforming Design for Hybrid-Duplex Wireless Backhaul Networks

Seok-Hyun Yoon, *Student Member, IEEE*, Byungju Lim, *Member, IEEE*, Mai Vu, *Senior Member, IEEE*, and Young-Chai Ko, *Senior Member, IEEE*

***Abstract*—The integration of a wireless backhaul network between a macro-cell base station (MBS) and multiple small-cell base stations (SBSs) with full-duplex (FD) technology at the SBSs offers significant potential to enhance spectrum efficiency in millimeter-wave (mmWave) communication systems. However, the FD mode also introduces an inherent trade-off between better time utilization and increased network interference, necessitating careful optimization of duplex modes at each SBS. In this paper, we propose a novel framework that jointly optimizes both the duplex mode selection for each SBS and the design of hybrid beamforming (BF) at the MBS and SBSs to maximize network throughput. Our framework alternately tackles two key subproblems: hybrid BF design and SBS duplex mode selection. For hybrid BF design, we employ a two-stage approach that combines a codebook-based radio frequency beam selection via a greedy algorithm with baseband BF optimization through a generalized power iteration method. For SBS duplex mode selection, we introduce the worst-mode switching (WMS) algorithm to efficiently find a near-optimal solution in polynomial time. Simulation results demonstrate that the proposed joint algorithm not only has low computational complexity but is also robust to various interference scenarios, including different ADC resolutions and varying levels of residual self-interference suppression. This adaptability results in superior sum-rate performance compared to conventional hybrid BF schemes and configurations where all SBSs operate exclusively in either full-duplex or half-duplex mode.**

***Index Terms*—Wireless backhual network, mmWave, hybrid-duplex, hybrid beamforming, duplex mode selection.**

I. Introduction

MILLIMETER-WAVE (mmWave) technologies have emerged as a key solution to meet the increasingly high data-rate requirements in 5G and beyond 5G (B5G) communication systems. However, due to the high path loss and sensitivity to obstacles, mmWave communications suffer from short ranges, which can be compensated by having a large number of antennas and utilizing beamforming (BF) techniques [1]. In addition, ultra-dense networks deploying numerous small-cell base stations (SBSs) offer a concurrent solution to increase network coverage. However, connecting these numerous SBSs to the core network through conventional wired fiber backhaul incurs substantial costs. In this regard, the wireless backhaul networks have been extensively researched in academia and industry. For example, the integrated access and backhaul (IAB) network was introduced in the 3rd Generation Partnership Project (3GPP) 5G Release 16, which is a promising architecture for improving connectivity and reducing cost in 5G [2]. Specifically, in an IAB network, an MBS connected to the core network via fiber cable establishes wireless backhaul links to the SBSs through a radio access network (RAN), sharing the same spectrum between backhaul and access links. This architecture reduces infrastructure costs and enables plug-and-play installation of SBSs. Motivated by these advantages, extensive research has been conducted on BF design [3], [4], performance analysis [5], and resource allocation [6], [7] in an mmWave IAB network.

Full-duplex (FD) communication is an emerging technology that can achieve up to twice the spectral efficiency compared to half-duplex (HD) communication [8]. Because of this advantage, the integration of FD communication and IAB networks, denoted as FD IAB, is recently considered in 3GPP Release 17 [9] for B5G and 6G systems. By enabling simultaneous transmission and reception on the backhaul and access links in the same time-frequency resource blocks, FD IAB can enhance data rates and reduce latency [10]. However, the main bottleneck in realizing FD IAB network is self-interference (SI), caused by the direct reception of a signal transmitted over an access link when receiving a desired signal from the backhaul link. The considerably higher power of the SI signal compared to the desired received signal and the noise floor results in ADC saturation and consequently degrades receiver performance, requiring an efficient SI cancellation (SIC) method.

A. Related Works

Research on SIC in sub-6GHz FD systems has been active over the past decade [11], [12], [13]. However, applying an analog domain SI cancellation (SIC) technique proposed for

Received 16 October 2024; revised 14 February 2025; accepted 27 March 2025. Date of publication 4 April 2025; date of current version 20 October 2025. This work was supported by institute of Information & Communications Technology Planning & Evaluation (IITP) under 6G-Cloud Research and Education Open Hub (IITP-2025-RS-2024-00428780) grant funded by the Korea government (MSIT). The associate editor coordinating the review of this article and approving it for publication was C. Pan. *(Corresponding authors: Byungju Lim; Mai Vu; Young-Chai Ko.)*

Seok-Hyun Yoon and Young-Chai Ko are with the School of Electrical Engineering, Korea University, Seoul 02841, South Korea (e-mail: daniel419@korea.ac.kr; koyc@korea.ac.kr).

Byungju Lim is with the Department of Electronic Engineering, Pukyong National University, Busan 48513, South Korea (e-mail: limbj@pknu.ac.kr).

Mai Vu is with the Department of Electrical and Computer Engineering, Tufts University, Medford, MA 02155 USA (e-mail: mai.vu@tufts.edu).

Digital Object Identifier 10.1109/TCOMM.2025.3557972

0090-6778 © 2025 IEEE. All rights reserved, including rights for text and data mining, and training of artificial intelligence and similar technologies. Personal use is permitted, but republication/redistribution requires IEEE permission.
See https://www.ieee.org/publications/rights/index.html for more information.

Authorized licensed use limited to: Univ Of Incheon. Downloaded on October 26,2026 at 13:17:40 UTC from IEEE Xplore. Restrictions apply.

sub-6GHz FD systems to mmWave FD systems is impractical due to the need for additional radio frequency (RF) hardware that scales with the number of antennas [14]. Instead, methods utilizing large-scale antenna arrays to spatially mitigate SI through BF have been recently proposed [15], [16], [17], [18], [19], [20]. For example, an orthogonal matching pursuit (OMP)-based hybrid BF SIC algorithm can mitigate SI and achieve high spectral efficiency in an mmWave FD relay system [15]. An RF BF scheme employs an alternating SI suppression algorithm for an mmWave FD unmanned aerial vehicle (UAV) relay system [16], and a hybrid BF SIC method works under practical scenario [17]. However, RF BF schemes for SI suppression as in [15], [16], and [17] are infeasible in practical mmWave systems since they require knowledge of the high-dimensional SI channel matrix. As such, recent research has focused on mitigating SI power using practical codebook-based RF BF [18], [19], [20]. For example, a DFT codebook is used to design hybrid BF [19] and a dynamic codebook for RF beams is employed using a reduction method [18] by restricting the SI power to prevent the saturation of low-noise amplifiers (LNAs) and analog-to-digital converters (ADCs). In addition, RF beam selection can be used to achieve high beamforming gain while significantly reducing SI [20].

The above existing works primarily focus on single-cell FD wireless backhaul networks, which cannot be directly extended to multi-cell networks due to challenges related to inter-cell interference. Although BF designs for multi-cell FD wireless backhaul networks have been explored in the sub-6 GHz band [21], [22], these algorithms are unsuitable for mmWave networks because they rely solely on baseband (BB) digital BF, leading to high costs and energy consumption.

To address complexity and hardware costs, a codebook-based RF BF SIC method can be used for mmWave multi-cell FD wireless backhaul networks [14], [18]. In this approach, each FD SBS selects RF beam sets that keep SI power within the ADC's dynamic range, preventing ADC saturation [19]. However, using codebook-based RF beams for SIC reduces the number of available RF beams in FD SBSs compared to HD SBSs. The reduction significantly limits the direct application of the codebook-based RF BF SIC method in mmWave multi-cell FD wireless backhaul networks. Beyond inter-backhaul interference and intra/inter-cell interference, FD multi-cell wireless backhaul networks also experience addtional interference, including inter-SBS and cross-tier interference. The limited number of available beams restricts the system's ability to simultaneously enhance user channel gain and mitigate interference power in FD systems. As a result, despite the potential to leverage additional time-frequency resources compared to HD systems, overall FD system performance deteriorates.

To mitigate these challenges, operating certain SBSs in HD mode while utilizing a larger number of RF beams can effectively eliminate SI and prevent additional interference caused by FD transmissions. Therefore, optimizing the duplex mode at each SBS and jointly designing hybrid BF are essential for improving system performance in mmWave FD wireless backhaul networks. However, existing works either do not consider beamforming [23] or assume fixed beamforming [24], [25] when optimizing the duplex mode. To the best of our knowledge, this issue has not been previously addressed and is examined for the first time in this work.

Several studies have demonstrated the benefits of adaptive duplex mode selection in hybrid FD/HD duplex cellular systems [23], [26], [27], [28], [29], [30], [31]. Duplex mode switching improve network throughput and coverage in heterogeneous networks (HetNets) with wireless backhaul [26]. A hybrid full-/half-duplex HetNet consisting of HD MBSs and FD SBSs can achieve high coverage probability and average spectral efficiency (SE) [27]. In addition,A cell association scheme and duplex mode selection strategy for hybrid full-/half-duplex two-tier HetNets which can enhance uplink SE for UEs [28]. A user scheduling scheme for wireless-powered hybrid full-/half-duplex HetNets demonstrates significant energy efficiency gains [29]. Duplex mode selection, when combined with resource allocation, can maximize network throughput [30], while optimizing transmit power further enhances network performance [31]. A self-backhauled FD network can also leverage duplex mode selection alongside power allocation to improve efficiency [23]. However, these works primarily focus on performance analysis, UE scheduling, and power allocation in sub-6GHz band. They do not consider the joint optimization of duplex mode and BF design in mmWave wireless backhaul systems, which remains an open research challenge.

Several prior works focus on selecting the duplex mode in network-assisted full-duplex (NAFD) cell-free (CF) networks [24], [25]. However, the solutions in these works have limitations for application in wireless backhaul networks due to the following reasons. Firstly, these works assume that all APs only operate in HD mode, while selecting either DL or UL mode. However, our work focuses on selecting FD or HD mode of each AP in wireless backhaul network. Secondly, while they consider fixed beamforming during duplex mode selection, our work jointly optimizes both the duplex mode and beamforming, accounting for the effects of beamforming on the selection of duplex mode. Thirdly, the operation mechanism of FD mode in CF network and wireless backhaul network is different. In the CF network, DL and UL access links operate in FD mode, while in wireless backhaul network, DL backhaul and DL access links operate in FD mode, leading to different signal models and the types of interference.

B. Our Contributions

As discussed above, despite the critical importance of dynamically selecting the duplex mode for each SBS and designing hybrid beamforming (BF) at the MBS and all SBSs, to the best of our knowledge, this issue has not been adequately addressed in the literature. In this paper, we propose a novel algorithm for hybrid beamforming design and duplex mode selection, marking the first study to address this joint problem in mmWave multi-cell hybrid FD/HD wireless backhaul networks. Our proposed joint algorithm effectively balances the trade-off between maximizing time resource utilization in FD mode and mitigating network interference in HD mode through the adaptive selection of the duplex mode for each

Authorized licensed use limited to: Univ Of Incheon. Downloaded on October 26,2026 at 13:17:40 UTC from IEEE Xplore. Restrictions apply.

SBS. The key contributions of this paper are summarized as follows.

- We consider an ADC saturation constraint for operating in an FD wireless backhaul network and define the transmit RF beam combination set for preventing the ADC saturation. We then integrate this constraint into a novel formulation to maximize the system sum rate by jointly designing the digital BF of the MBS and the hybrid BF of all SBSs, together with selecting the duplex mode for each SBS. To address this NP-hard problem, we propose an novel optimization framework to alternately solve two subproblems, the hybrid BF design and the duplex mode selection.
- For fixed SBS duplex modes, we propose a two-stage hybrid BF design algorithm. In the first stage, we introduce a codebook-based greedy RF beam-user pair selection algorithm to maximize a lower bound on the throughput of access link at each SBS. This algorithm can effectively mitigate inter-SBS (inter-cell) interference in the beam domain in a distributed manner with low complexity, ensuring minimum performance. In the second stage, we optimize the baseband BF by reformulating the optimization problem as an eigenvector-dependent nonlinear eigenvalue problem, which can be solved by utilizing the generalized power iteration (GPI) algorithm. Through this two-stage process, we can jointly optimize the baseband BF of MBS and hybrid BF of the SBSs, providing a good local optimal solution.
- We propose an efficient algorithm, called worst mode switching (WMS), for the duplex mode selection of each SBS, which converges to a near-optimal solution in polynomial time. By iteratively switching the duplex mode of the SBS cell with worst data rate, the proposed algorithm can improve the data rate by utilizing more time resources and reducing interference from other SBSs.
- Numerical results demonstrate that the proposed joint algorithm approaches the performance of exhaustive search and outperforms the case when all SBSs operate in either FD or HD, as well as other hybrid BF benchmark schemes. These numerical results illustrate that dynamic duplex mode selection can efficiently control network interference by dynamically selecting the duplex mode while considering SBS transmit power, SIC errors, and ADC resolutions.

The rest of this paper is organized as follows. In Section II, we present the system model of a mmWave hybrid FD/HD system. We formulate the joint hybrid BF and duplex mode optimization problem in Section III. Next, we propose the two stage hybrid BF design algorithm and the duplex mode selection algorithm in Section IV and Section V, respectively. Section VI presents numerical results to evaluate performance of the proposed algorithms, and we conclude in Section VII.

Notation: x is a scalar; $\mathbf{x}$ is a column vector; $\mathbf{X}$ is a matrix; $(\cdot)^*$, $(\cdot)^{\mathsf{T}}$, $(\cdot)^{\mathsf{H}}$, and $(\cdot)^{-1}$ denote the conjugate, transpose, Hermitian and matrix inversion, respectively; $\mathbf{I}_M$ is an identity matrix of size $M \times M$; $[\mathbf{X}]_{n,m}$ denotes the element at the nth row and the mth column of matrix $\mathbf{X}$; $\mathbf{e}_k$ denotes $\|\mathbf{x}\|$ denotes l_2-norm of a vector $\mathbf{x}$; $\mathsf{blkdiag}(\mathbf{X}_1, \cdots, \mathbf{X}_N)$ is a block-diagonal matrix concatenating matrices $\mathbf{X}_1, \cdots, \mathbf{X}_N$; $\mathbf{e}_l$ is a unit vector with the nonzero value in the l-th element; $|\mathcal{X}|$ denotes the cardinality of set $\mathcal{X}$; $\otimes$ denotes the Kronecker product; $\mathcal{O}(\cdot)$ denotes big-O for describing complexity orders.

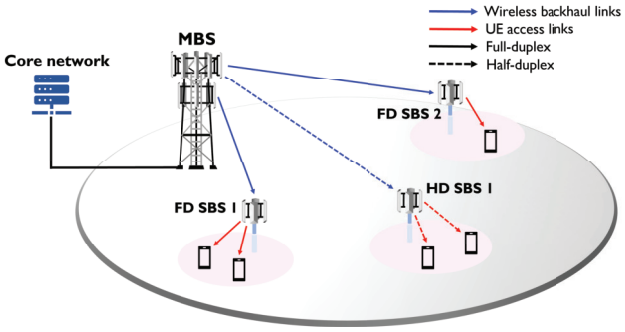


Fig. 1. Two-tier mmWave multi-cell hybrid duplex wireless backhaul network.

II. System Model

A. Network Model

We consider a two-tier mmWave multi-cell downlink wireless backhaul network, where a MBS (i.e., IAB donor) connected to a core network provides wireless backhaul links to L distributed SBSs (i.e., IAB nodes). Each SBS serves K single-antenna UEs via wireless access links. Each SBS can select either FD mode or time-division duplex (TDD) HD mode for hybrid-duplex system. When SBS operates in FD mode, it transmits access link signals to UEs while receiving backhaul link signals from the MBS using the same time-frequency resource. When SBS operates in HD mode with TDD, the reception of backhaul link signals and the transmission of access link are performed in different time resources. We denote the index of MBS as 0, and the set of SBSs as $\mathcal{L} \triangleq \{1, 2, \ldots, L\}$. The MBS and SBSs are implemented by a fully-connected hybrid BF structure. Specifically, the MBS is equipped with N^{d} transmit antennas and $N^{\mathsf{d}}_{\mathsf{RF}}$ RF chains such that $L = N^{\mathsf{d}}_{\mathsf{RF}} \leq N^{\mathsf{d}}$. Each SBS is equipped with separate multi-panel antennas [32], [33], where one panel with N^{r} antennas is used for establishing backhaul link and the another panel with N^{t} antennas is used for establishing the access link. In this multi-panel structure, antennas and RF chains for backhaul and access links are installed separately to enhance the performance of each link and mitigate self-interference in the propagation domain by physically and spatially separating the backhaul link panel and the access link panel. In our work, we assume this multi-panel structure in SBS, but the proposed algorithm is not limited to the multi-panel structure and can be also applicable to single-panel structure. In addition, the number of transmit and receive RF chains for each SBS is denoted as $N^{\mathsf{t}}_{\mathsf{RF}}$ and $N^{\mathsf{r}}_{\mathsf{RF}}$ such that $K = N^{\mathsf{t}}_{\mathsf{RF}} \leq N^{\mathsf{t}}$ and $N^{\mathsf{r}}_{\mathsf{RF}} \leq N^{\mathsf{r}}$. We assume that MBS and SBSs are configured in a uniform planar array (UPA) structure parallel to the y-z plane. In this UPA structure, the number of antenna elements in the horizontal and vertical directions is N^x_1 and N^x_2, respectively, with $N^x = N^x_1 N^x_2$, where $x \in \{\mathsf{d}, \mathsf{t}, \mathsf{r}\}$. This network model is illustrated in Fig. 1.

Authorized licensed use limited to: Univ Of Incheon. Downloaded on October 26,2026 at 13:17:40 UTC from IEEE Xplore. Restrictions apply.

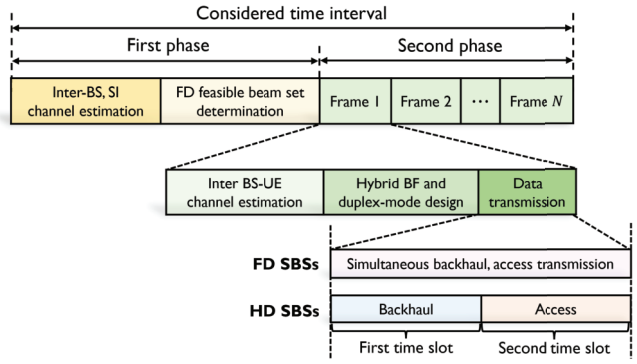


Fig. 2. Frame structure of the protocol for hybrid-duplex wireless backhaul.

To maintain stable connectivity for the backhaul link, all the MBS and SBSs should be installed at a relatively higher position than other obstacles in the city. Moreover, a LoS path is dominant in the channel between BSs [3], [34], and thereby the inter-BS channel can be considered as a static over a long-term period. Furthermore, the SI channel of each SBS remains relatively stable due to direct coupling between the arrays. In this paper, we focus on a specific time interval when these channels remain constant, as shown in Fig. 2.

The considered time interval can be divided into two phases. In the first phase, the beam-domain channel state information (CSI) of inter-BS and SI channels are estimated using existing channel estimation and feedback methods [35]. By leveraging the characteristics of the static inter-BS and SI channels, these channels can be estimated only once during the long-term period, and the CSIs of these channels can be used in the second phase for each frame, leading to a reduction in channel estimation and feedback overhead. Then, based on the estimated CSI of its SI channel, each SBS determines the candidate RF beam set for FD transmission. The second phase is composed of multiple frames, each of which corresponds to the coherence time of the BS-UE channel. Since the BS-UE channel is time-varying due to UE mobility, the beam domain CSIs of the MBS-UE channels and SBS-UE channels are estimated in every frame. Utilizing the estimated CSI, the MBS designs its hybrid BF and each SBS determines its duplex mode and also designs its hybrid BF matrices for the backhaul and access links to maximize the network sum rate. Depending on the duplex mode, backhaul link and access link are operated either sequentially or simultaneously during two time slots.

B. Channel Model

We adopt a distance-dependent path loss model, given by

$$\xi_y(d)_{[\mathrm{dB}]} = a_y + 20\log_{10}(f_c) + 10b_y\log_{10} d_{[\mathrm{m}]} + \chi_y \quad (1)$$

where f_c is the carrier frequency in GHz, a_y is the reference path loss at a distance of 1m and $\chi_y \sim \mathcal{CN}(0,\sigma_y^2)$ is the log-normal shadow fading.[1] Note that $y \in \{\mathsf{L},\mathsf{N}\}$, where L and N denote LoS and NLoS, respectively. Furthermore, the small-scale fading channels, $\mathbf{H}_{j,l}^{\mathsf{L}}$ and $\mathbf{H}_{j,l}^{\mathsf{N}}$, from the j-th BS to the l-th BS, and $\mathbf{g}_{j,l,k}^{\mathsf{L}}$ and $\mathbf{g}_{j,l,k}^{\mathsf{N}}$, from the j-th BS to the k-th UE associated with the l-th BS, for LoS and NLoS paths, are given respectively as

$$\begin{aligned}
\mathbf{H}_{j,l}^{\mathsf{L}} &= \alpha_{j,l}^{\mathsf{L}}\mathbf{a}(\varphi_{j,l}^{a,\mathsf{L}},\varphi_{j,l}^{e,\mathsf{L}})\mathbf{a}^{\mathsf{H}}(\vartheta_{j,l}^{a,\mathsf{L}},\vartheta_{j,l}^{e,\mathsf{L}}),\\
\mathbf{H}_{j,l}^{\mathsf{N}} &= \frac{1}{\sqrt{N^{\mathsf{p}}}}\sum_{p=1}^{N^{\mathsf{p}}}\alpha_{j,l,p}^{\mathsf{N}}\mathbf{a}(\varphi_{j,l,p}^{a,\mathsf{N}},\varphi_{j,l,p}^{e,\mathsf{N}})\mathbf{a}^{\mathsf{H}}(\vartheta_{j,l,p}^{a,\mathsf{N}},\vartheta_{j,l,p}^{e,\mathsf{N}}),\\
\mathbf{g}_{j,l,k}^{\mathsf{L}} &= \alpha_{j,l,k}^{\mathsf{L}}\mathbf{a}^{\mathsf{H}}(\vartheta_{j,l,k}^{a,\mathsf{L}},\vartheta_{j,l,k}^{e,\mathsf{L}}),\\
\mathbf{g}_{j,l,k}^{\mathsf{N}} &= \frac{1}{\sqrt{N^{\mathsf{p}}}}\sum_{p=1}^{N^{\mathsf{p}}}\alpha_{j,l,k,p}^{\mathsf{N}}\mathbf{a}^{\mathsf{H}}(\vartheta_{j,l,k,p}^{a,\mathsf{N}},\vartheta_{j,l,k,p}^{e,\mathsf{N}}),
\end{aligned} \quad (2)$$

where $\alpha_{j,l}^{a,\mathsf{L}}$ and $\alpha_{j,l,p}^{a,\mathsf{N}}$ denote the small scale gains of the LoS path and the p-th NLoS path from the j-th BS to the l-th BS, while $\alpha_{j,l,k}^{a,\mathsf{L}}$ and $\alpha_{j,l,k,p}^{a,\mathsf{N}}$ denote the small scale gains of the LoS path and the p-th NLoS path from the j-th BS to the k-th UE associated with the l-th BS, respectively. These complex path gains follow the circularly symmetric complex Gaussian (CSCG) distribution with zero mean and unit variance. In addition, in the channels from the j-th BS to the l-th BS, $\varphi_{j,l}^{a,\mathsf{L}}$ ($\varphi_{j,l}^{e,\mathsf{L}}$) and $\varphi_{j,l,p}^{a,\mathsf{N}}$ ($\varphi_{j,l,p}^{e,\mathsf{N}}$) denote the azimuth (elevation) AoA of the LoS path and the p-th NLoS path, while $\vartheta_{j,l}^{a,\mathsf{L}}$ ($\vartheta_{j,l}^{e,\mathsf{L}}$) and $\vartheta_{j,l,p}^{a,\mathsf{N}}$ ($\vartheta_{j,l,p}^{e,\mathsf{N}}$) denote the azimuth (elevation) AoD for the LoS path and the p-th NLoS path, respectively. Similarly, in the channels from the j-th BS to the k-th UE associated with the l-th BS, $\varphi_{j,l,k}^{a,\mathsf{L}}$ ($\varphi_{j,l,k}^{e,\mathsf{L}}$) and $\varphi_{j,l,k,p}^{a,\mathsf{N}}$ ($\varphi_{j,l,k,p}^{e,\mathsf{N}}$) denote the azimuth (elevation) AoA of the LoS path and the p-th NLoS path, while $\vartheta_{j,l,k}^{a,\mathsf{L}}$ ($\vartheta_{j,l,k}^{e,\mathsf{L}}$) and $\vartheta_{j,l,k,p}^{a,\mathsf{N}}$ ($\vartheta_{j,l,k,p}^{e,\mathsf{N}}$) denote the azimuth (elevation) AoD of the LoS path and p-th NLoS path, respectively.[2] The number of NLoS paths is denoted as N^{p}. For the UPA structure, the array response vector is defined as

$$\begin{aligned}
\mathbf{a}(\phi,\theta) = \big[1,\cdots,e^{j\pi(u\cos(\theta)\sin(\phi)+v\sin(\theta))},\cdots,\\
e^{j\pi((N_1^x-1)\cos(\theta)\sin(\phi)+(N_2^x-1)\sin(\theta))}\big]^{\mathsf{T}},
\end{aligned} \quad (3)$$

where $u \in [0,\cdots,N_1^x-1]$ and $v \in [0,\cdots,N_2^x-1]$ are the indices of antenna elements in horizontal and vertical direction, respectively.

Considering the specific characteristics of mmWave propagation, such as high path loss, directivity, and a limited number of scatters, we adopt a narrowband geometric channel model as modeled in [18]. For the backhaul links, we assume that a LoS path is always guaranteed and its path gain is significantly higher than that of NLoS paths due to the high installation elevation of the MBS. Thus, we can ignore NLoS paths in the backhaul link. Then, the backhaul link channel from MBS to the l-th SBS can be expressed as $\mathbf{H}_{0,l} = \sqrt{\xi_{\mathsf{L}}(d_{0,l})}\mathbf{H}_{0,l}^{\mathsf{L}}$, where $d_{0,l}$ is the distance between the MBS and the l-th SBS.

For the channels between SBSs, both LoS and NLoS paths exist, thus the channel from the j-th SBS to the l-th SBS is

[1]Path loss parameters are determined by the type of BS at $f_c = 28$GHz. For MBS, $\alpha_{\mathsf{L}} = 28$,$\beta_{\mathsf{L}} = 2.2$,$\sigma_{\mathsf{L}}^2 = 4$dB,$\alpha_{\mathsf{N}} = 32.4$,$\beta_{\mathsf{N}} = 3$ and $\sigma_{\mathsf{N}}^2 = 7.8$dB; while for SBS, $\alpha_{\mathsf{L}} = 32.4$,$\beta_{\mathsf{L}} = 2.1$,$\sigma_{\mathsf{L}}^2 = 4$dB,$\alpha_{\mathsf{N}} = 32.4$,$\beta_{\mathsf{N}} = 3.19$ and $\sigma_{\mathsf{N}}^2 = 8.2$dB [36].

[2]By exploiting pilot signals, the conventional algorithms such as multiple signal classification (MUSIC) [37] or estimation of signal parameters via rotational invariant techniques (ESPIRIT) [38] can be applied to estimate the AoD or AoA of each path in mmWave channels.

Authorized licensed use limited to: Univ Of Incheon. Downloaded on October 26,2026 at 13:17:40 UTC from IEEE Xplore. Restrictions apply.

expressed as $\mathbf{H}_{j,l} = \sqrt{\xi_{\mathsf{L}}(d_{j,l})}\mathbf{H}^{\mathsf{L}}_{j,l} + \sqrt{\xi_{\mathsf{N}}(d_{j,l})}\mathbf{H}^{\mathsf{N}}_{j,l}$, where $d_{j,l}$ is the distance between the j-th SBS and the l-th SBS. For the channels from the BSs to the UEs, the existence of a LoS path cannot be guaranteed due to the random locations of the UE and potential obstacles. Therefore, we adopt a probabilistic LoS mmWave channel model, and the channel from the i-th BS to the k-th UE associated with the l-th SBS is expressed as $\mathbf{g}_{i,l,k} = U_{i,l,k}\sqrt{\xi_{\mathsf{L}}(d_{i,l,k})}\mathbf{g}^{\mathsf{L}}_{i,l,k} + \sqrt{\xi_{\mathsf{N}}(d_{i,l,k})}\mathbf{g}^{\mathsf{N}}_{i,l,k}$, $i \in \{0\} \cup \mathcal{L}$, where $d_{i,l,k}$ is the distance between the i-th BS and the k-th UE associated with the l-th SBS, and $U_{i,l,k}$ is a Bernoulli random variable with the LoS probability $\mathrm{P}_{\mathsf{LoS}}(d_{i,l,k})$ [3].

For FD mode, the SI channel must be considered. Since the distance between the transmit and receive panels in a SBS is very close, the LoS SI channel does not satisfy the conventional far-field planar channel model. Instead, a spherical wave model has been used for the SI channel [39]. Based on this model, the LoS SI channel of the l-th SBS is given by

$$[\mathbf{H}^{\mathsf{SI,L}}_l]_{mn} = \sqrt{\xi_{\mathsf{LoS}}(d^{mn}_l)}\,\exp\left(-j2\pi\frac{d^{mn}_l}{\lambda}\right). \tag{4}$$

where d^{mn}_l is the distance between the n-th transmit antenna and m-th receive antenna of the l-th SBS and λ is the carrier wavelength. For the NLoS SI channel, we assume a far-field planar wave due to reflections in nearby scatters, which is modeled as in (2). Then, the complete SI channel of the l-th SBS is expressed as $\mathbf{H}^{\mathsf{SI}}_l = \mathbf{H}^{\mathsf{SI,L}}_l + \sqrt{\xi_{\mathsf{N}}(d_l)}\mathbf{H}^{\mathsf{SI,N}}_l$, where d_l is the distance between transmit and receive antenna arrays of the l-th SBS.

C. Signal Model

In the backhaul links, the MBS transmits a single data stream to each SBS using a hybrid BF denoted as $\mathbf{F} = \mathbf{F}^{\mathsf{RF}}\mathbf{F}^{\mathsf{BB}} \in \mathbb{C}^{N^{\mathsf{d}}\times L}$, which must satisfy the power constraint $\|\mathbf{F}\|^2_{\mathrm{F}} \le 1$. The RF BF matrix, consisting of phase shifters with constant magnitude, is denoted as $\mathbf{F}^{\mathsf{RF}} \in \mathbb{C}^{N^{\mathsf{d}}\times L}$, and the baseband (BB) BF matrix is denoted as $\mathbf{F}^{\mathsf{BB}} = [\mathbf{f}^{\mathsf{BB}}_1|\mathbf{f}^{\mathsf{BB}}_2|\cdots|\mathbf{f}^{\mathsf{BB}}_L] \in \mathbb{C}^{L\times L}$. The receive RF BF vector of the l-th SBS is denoted as $\mathbf{v}_l \in \mathbb{C}^{N^{\mathsf{r}}\times 1}$ with the assumption of $N^{\mathsf{r}}_{\mathsf{RF}} = 1$.

In the access links, the l-th SBS transmits a single data stream to each associated UE simultaneously using the hybrid BF denoted as $\mathbf{W}_l = \mathbf{W}^{\mathsf{RF}}_l\mathbf{W}^{\mathsf{BB}}_l \in \mathbb{C}^{N^{\mathsf{t}}\times K}$, satisfying the power constraint $\|\mathbf{W}_l\|^2_{\mathrm{F}} \le 1$. The RF BF matrix of the l-th SBS is denoted as $\mathbf{W}^{\mathsf{RF}}_l = [\mathbf{w}^{\mathsf{RF}}_{l,1}|\mathbf{w}^{\mathsf{RF}}_{l,2}|\cdots|\mathbf{w}^{\mathsf{BB}}_{l,K}] \in \mathbb{C}^{N^{\mathsf{t}}\times K}$. The BB BF matrix is denoted as $\mathbf{W}^{\mathsf{BB}}_l = [\mathbf{w}^{\mathsf{BB}}_{l,1}|\mathbf{w}^{\mathsf{BB}}_{l,2}|\cdots|\mathbf{w}^{\mathsf{BB}}_{l,K}] \in \mathbb{C}^{K\times K}$.

To represent the duplex mode selection of each SBS, we define the binary selection indicator $\boldsymbol{\lambda} = [\lambda_1, \lambda_2, \cdots, \lambda_L]^{\mathsf{T}}$, where λ_l satisfies the following conditions

$$\lambda_l = \begin{cases} 1, & \text{if the l-th SBS operates in FD mode,} \\ 0, & \text{if the l-th SBS operates in HD mode.} \end{cases} \tag{5}$$

[3]The LoS probability is dependent on the distance, and is defined in 3GPP standard as $\mathrm{P}_{\mathsf{LoS}}(d) = 1$ if $d \le 18\mathrm{m}$ and $\mathrm{P}_{\mathsf{LoS}}(d) = \frac{18}{d} + \exp\left(-\frac{d}{36}\right)\left(1-\frac{18}{d}\right)$ if $d > 18\mathrm{m}$ [36].

1) Backhaul Link Signal Model: In the first time slot at each frame, the received backhaul signal at SBS can be affected by inter-backhaul interference (IBI), inter-SBS interference (ISI) from FD SBSs, and self-interference (SI). Accordingly, the received signal at the l-th SBS in the first time slot can be expressed as

$$\begin{aligned} y^{\mathsf{B},1}_l = {} & \underbrace{\mathbf{v}^{\mathsf{H}}_l\mathbf{H}_{0,l}\mathbf{F}^{\mathsf{RF}}\mathbf{f}^{\mathsf{BB}}_l s^{\mathsf{B},1}_l}_{\text{desired signal}} + \underbrace{\sum_{j\neq l}^{L}\mathbf{v}^{\mathsf{H}}_l\mathbf{H}_{0,l}\mathbf{F}^{\mathsf{RF}}\mathbf{f}^{\mathsf{BB}}_j s^{\mathsf{B},1}_j}_{\text{inter-backhaul interference}} \\ & + \underbrace{\sum_{j\neq l}^{L}\sum_{m=1}^{K}\lambda_j\mathbf{v}^{\mathsf{H}}_l\mathbf{H}_{j,l}\mathbf{W}^{\mathsf{RF}}_j\mathbf{w}^{\mathsf{BB}}_{j,m}s^{\mathsf{A},1}_{j,m}}_{\text{inter-SBS interference}} \\ & + \underbrace{\sum_{m=1}^{K}\lambda_l\mathbf{v}^{\mathsf{H}}_l\mathbf{H}^{\mathsf{SI}}_l\mathbf{W}^{\mathsf{RF}}_l\mathbf{w}^{\mathsf{BB}}_{l,m}s^{\mathsf{A},1}_{l,m}}_{\text{self-interference}} + \underbrace{\mathbf{v}^{\mathsf{H}}_l\mathbf{n}^{\mathsf{B},1}_l}_{\text{noise}}, \end{aligned} \tag{6}$$

where $s^{\mathsf{B},1}_l \sim \mathcal{CN}(0, P_{\mathsf{B}})$ and $s^{\mathsf{A},1}_{l,m} \sim \mathcal{CN}(0, P_{\mathsf{A}})$ are backhaul link symbol for the l-th SBS and access link symbol for the m-th UE associated with the l-th SBS in the first time slot, respectively, with the MBS maximum transmit power P_{B} and the SBS maximum transmit power P_{A}, and $\mathbf{n}^{\mathsf{BH},1}_l \sim \mathcal{CN}(0, \sigma^2\mathbf{I}_{N^{\mathsf{r}}})$ is the additive white Gaussian noise (AWGN) with noise power σ^2.

In the second time slot at each frame, the received backhaul signal of FD SBS is affected by IBI, ISI from other FD SBSs, and SI. On the other hand, HD SBS does not receive desired backhaul signal. Therefore, the received signal at the l-th SBS in the second time slot can be expressed as

$$\begin{aligned} y^{\mathsf{B},2}_l = \lambda_l\Big(& \underbrace{\mathbf{v}^{\mathsf{H}}_l\mathbf{H}_{0,l}\mathbf{F}^{\mathsf{RF}}\mathbf{f}^{\mathsf{BB}}_l s^{\mathsf{B},2}_l}_{\text{desired signal}} + \underbrace{\sum_{j\neq l}^{I}\lambda_j\mathbf{v}^{\mathsf{H}}_l\mathbf{H}_{0,l}\mathbf{F}^{\mathsf{RF}}\mathbf{f}^{\mathsf{BB}}_j s^{\mathsf{B},2}_j}_{\text{inter-backhaul interference}} \\ & + \underbrace{\sum_{j\neq l}^{L}\sum_{m=1}^{K}\mathbf{v}^{\mathsf{H}}_l\mathbf{H}_{j,l}\mathbf{W}^{\mathsf{RF}}_j\mathbf{w}^{\mathsf{BB}}_{j,m}s^{\mathsf{A},2}_{j,m}}_{\text{inter-SBS interference}} \\ & + \underbrace{\sum_{m=1}^{K}\mathbf{v}^{\mathsf{H}}_l\mathbf{H}^{\mathsf{SI}}_l\mathbf{W}^{\mathsf{RF}}_l\mathbf{w}^{\mathsf{BB}}_{l,m}s^{\mathsf{A},2}_{l,m}}_{\text{self-interference}} + \underbrace{\mathbf{v}^{\mathsf{H}}_l\mathbf{n}^{\mathsf{B},2}_l}_{\text{noise}}\Big). \end{aligned} \tag{7}$$

2) Access Link Signal Model: In the first time slot at each frame, the received signal at the UE associated with a FD SBS is affected by inter-UE interference (IUI), and inter-cell interference (ICI) from other FD SBSs as well as cross-tier interference (CTI) from MBS. Note that in the first time slot, FD SBSs only transmit data to their associated UEs while SBSs with a HD mode are not involved. Accordingly, the received signal at the k-th UE associated with the l-th SBS in the first time slot can be expressed as

$$y^{\mathsf{A},1}_{l,k} = \lambda_l\Big(\underbrace{\mathbf{g}_{l,l,k}\mathbf{W}^{\mathsf{RF}}_l\mathbf{w}^{\mathsf{BB}}_{l,k}s^{\mathsf{A},1}_{l,k}}_{\text{desired signal}} + \underbrace{\sum_{j=1}^{L}\mathbf{g}_{0,l,k}\mathbf{F}^{\mathsf{RF}}\mathbf{f}^{\mathsf{BB}}_j s^{\mathsf{B},1}_j}_{\text{cross-tier interference}}$$

Authorized licensed use limited to: Univ Of Incheon. Downloaded on October 26,2026 at 13:17:40 UTC from IEEE Xplore. Restrictions apply.

$$+\underbrace{\sum_{m\neq k}^{K}\mathbf{g}_{l,l,k}\mathbf{W}_l^{\mathsf{RF}}\mathbf{w}_{l,m}^{\mathsf{BB}}s_{l,m}^{\mathsf{A},1}}_{\text{intra-cell interference}}$$
$$+\underbrace{\sum_{j\neq l}^{L}\sum_{m=1}^{K}\lambda_j\mathbf{g}_{j,l,k}\mathbf{W}_j^{\mathsf{RF}}\mathbf{w}_{j,m}^{\mathsf{BB}}s_{j,m}^{\mathsf{A},1}}_{\text{inter-cell interference}}+\underbrace{n_{l,k}^{\mathsf{A},1}}_{\text{noise}}\Big), \quad (8)$$

In the second time slot of each frame, the received access signal at UE is affected by IUI, and ICI from other FD SBSs, as well as CTI from MBS. Therefore, the received signal at the k-th UE associated with the l-th SBS in the second time slot can be expressed as

$$y_{l,k}^{\mathsf{A},2}=\underbrace{\mathbf{g}_{l,l,k}\mathbf{W}_l^{\mathsf{RF}}\mathbf{w}_{l,k}^{\mathsf{BB}}s_{l,k}^{\mathsf{A},2}}_{\text{desired signal}}+\underbrace{\sum_{j=1}^{L}\lambda_j\mathbf{g}_{0,l,k}\mathbf{F}^{\mathsf{RF}}\mathbf{f}_j^{\mathsf{BB}}s_j^{\mathsf{B},2}}_{\text{cross-tier interference}}$$
$$+\underbrace{\sum_{m\neq k}^{K}\mathbf{g}_{l,l,k}\mathbf{W}_l^{\mathsf{RF}}\mathbf{w}_{l,m}^{\mathsf{BB}}s_{l,m}^{\mathsf{A},2}}_{\text{intra-cell interference}}$$
$$+\underbrace{\sum_{j\neq l}^{L}\sum_{m=1}^{K}\mathbf{g}_{j,l,k}\mathbf{W}_j^{\mathsf{RF}}\mathbf{w}_{j,m}^{\mathsf{BB}}s_{j,m}^{\mathsf{A},2}}_{\text{inter-cell interference}}+\underbrace{n_{l,k}^{\mathsf{A},2}}_{\text{noise}}. \quad (9)$$

We note that selecting the duplex mode of each SBS can significantly impact various interference terms of the received backhaul and access link signals in each time slot. The MBS transmits the backhaul link signals to all SBSs in the first time slot, while it transmits signals only to the SBSs operating in FD mode in the second time slot. Therefore, λ_j is not included in the IBI term of (6) and the CTI term of (8), whereas the IBI term of (7) and the CTI term of (9) includes λ_j. In addition, in the first time slot, only SBSs operating in FD mode transmit the access link signals, which results in λ_j being included in the ISI term of (6) and the ICI term of (8). However, since all SBSs transmit the access link signals in the second time slot, λ_j is not included in the ISI term of (7) and the ICI term of (9). As observed in (6)–(9), the duplex mode selection significantly affects the amount of interference, and thus a hybrid-duplex wireless backhaul network can achieve a better network performance than existing all-FD or all-HD wireless backhaul networks which cannot adjust the duplex mode based on the level of interference.

3) Digital Self-Interference Cancellation (D-SIC) Model: With the designed RF BF of the SBS, $\mathbf{W}_l^{\mathsf{RF}}$, each FD SBS is able to estimate the beam-domain SI channel by standard estimation methods [35]. After estimation, we can express the perfect beam-domain SI channel of the l-th SBS as the sum of the estimated beam-domain SI channel and the estimation error vector $\mathbf{\Delta}_{l,\mathsf{SI}}$, given as

$$\mathbf{v}_l^{\mathsf{H}}\mathbf{H}_{l,l}\mathbf{W}_l^{\mathsf{RF}}=\mathbf{h}_{l,\mathsf{eff}}^{\mathsf{H}}+\mathbf{\Delta}_{l,\mathsf{SI}}^{\mathsf{H}},\ \mathbf{\Delta}_{l,\mathsf{SI}}\sim\mathcal{CN}(\mathbf{0},\sigma_{\mathsf{SI}}^2\mathbf{I}), \quad (10)$$

By utilizing conventional digital self-interference cancellation (D-SIC) methods as in [40], we can effectively cancel out $\mathbf{h}_{l,\mathsf{eff}}^{\mathsf{H}}$. Consequently, the residual SI signal of the l-th SBS at the u-th time slot can be written as

$$y_l^{\mathsf{RSI},u}=\sum_{m=1}^{K}\lambda_l\mathbf{\Delta}_{l,\mathsf{SI}}^{\mathsf{H}}\mathbf{w}_{l,m}^{\mathsf{BB}}s_{l,m}^{\mathsf{A},u},\ u\in\{1,2\}, \quad (11)$$

Based on (6)–(11), the signal-to-interference-plus-ratio (SINR) of the l-th SBS and the k-th UE associated with the l-th SBS in the first and the second time slots are given in (12)-(15), as shown at the bottom of the next page. Given the perfect CSIs of effective backhaul channel, $\mathbf{v}_l^{\mathsf{H}}\mathbf{H}_{0,l}\mathbf{F}^{\mathsf{RF}}\mathbf{f}_l^{\mathsf{BB}}$ and effective access channel, $\mathbf{g}_{l,l,k}\mathbf{W}_l^{\mathsf{RF}}\mathbf{w}_{l,k}^{\mathsf{BB}}$, an upper bound for the achievable rates of backhaul link of the l-th SBS and access link of the k-th UE served by the l-th SBS can be written as

$$R_l^{\mathsf{B}}=\tau\log_2(1+\gamma_l^{\mathsf{B},1})+(1-\tau)\log_2(1+\gamma_l^{\mathsf{B},2}), \quad (16)$$
$$R_{l,k}^{\mathsf{A}}=\tau\log_2(1+\gamma_{l,k}^{\mathsf{A},1})+(1-\tau)\log_2(1+\gamma_{l,k}^{\mathsf{A},2}), \quad (17)$$

where $\tau\in[0,1]$ is the portion of time resource allocated for the first time slot. In this work, we assume $\tau=0.5$ to make equal time intervals for backhaul and access transmissions.[4] Since the end-to-end rate for each SBS cell can be determined by the minimum of the backhaul link rate and sum of the access link rates for all the UEs, the total achievable rate in a network is expressed as

$$R^{\mathsf{sum}}=\sum_{l=1}^{I}\min\left\{R_l^{\mathsf{B}},\sum_{k=1}^{K}R_{l,k}^{\mathsf{A}}\right\}. \quad (18)$$

In a HetNet, the data rate of backhaul link must be no less than the sum rate of all the access links. Therefore, we define the objective function as the minimum of the backhaul link rate and the sum rate of all the access links. Since the backhaul and access links are highly coupled by sharing the same wireless resources and affecting interference with each other, we should find an optimal solution of duplex mode and hybrid BF to strike a balance between the backhaul link rate and the access link rate.

III. Problem Formulation

Generally speaking, applying analog SIC, whose cost and complexity are proportional to the number of antennas, to FD mmWave systems is challenging. Instead, directional RF beams, enabled by the large-scale antennas, can be used to reduce SI power while ADC saturation is prevented. Therefore, in this section, we first determine a set of feasible RF beam combinations which satisfy the ADC dynamic range constraints. Based on this set, we construct an FD RF beam codebook for the transmission of FD SBSs. Next, we formulate the optimization problem to find the optimal solutions of hybrid BF at MBS and SBSs, and the duplex mode of each SBS which maximizes the sum rate.

[4]In addition, τ can be also optimized to enhance network performance, but our primary objective is to optimize duplex mode selection and hybrid BF to understand their impacts on the total achievable rate of IAB network. Optimizing τ is not addressed in this work, however, it can be a topic for future research.

Authorized licensed use limited to: Univ Of Incheon. Downloaded on October 26,2026 at 13:17:40 UTC from IEEE Xplore. Restrictions apply.

A. Construction of FD RF Beam Combination Set

In a practical system with low implementation complexity, HD mmWave systems select the transmit and the receive RF beams from the predefined codebook. These selected beams are chosen for providing high beamforming gains at the respective transmit and receive links, compensating for the high path loss. However, in FD mmWave systems, the SI should be considered when selecting beams as well, since the transmit and the receive beams are highly coupled through the SI channel. Specifically, the excessive power of SI can cause ADC saturation, resulting in degradation in the quality of the desired receive signal. Therefore, it is crucial to select the transmit-receive beam pairs that effectively mitigate a large portion of SI while ensuring that the residual SI power falls within the dynamic range of ADC [41]. In [18] and [19], the specific RF beam condition to prevent ADC saturation are driven for the l-th SBS as

$$\sum_{k=1}^{K} \frac{P_{\mathsf{A}}}{\sigma^2} \left|\mathbf{v}_l^{\mathsf{H}} \mathbf{H}_{l,l} \mathbf{w}_{l,k}^{\mathsf{RF}}\right|^2 \leq \eta_{\mathsf{ADC}}, \tag{19}$$

where η_{ADC} represents the power threshold of a B bit ADC resolution determined by its dynamic range as

$$\eta_{\mathsf{ADC}} = 6.021 \cdot B + 1.763 - 10\,(\mathrm{dB}), \tag{20}$$

To prevent RF saturation, the transmit RF beams $\mathbf{w}_{l,k}^{\mathsf{RF}}$ and the receive RF beam $\mathbf{v}_l^{\mathsf{RF}}$ of an FD SBS are designed to satisfy (19). The set of the feasible transmit and receive beam combinations, denoted as $\mathcal{A}_l^{\mathsf{FD}}$, should be periodically updated at each time interval as shown in Fig. 2. This update involves searching for all the combinations of beams included in the existing HD transmit and receive beam codebooks $\mathcal{W}_l^{\mathsf{HD}}$ and $\mathcal{V}_l^{\mathsf{HD}}$. Due to slow variation of the SI channel, each SBS can update its FD beam set during a long-term period, resulting in low overhead. Then, the FD codebooks $\mathcal{W}_l^{\mathsf{FD}}$ and $\mathcal{V}_l^{\mathsf{FD}}$ can be constructed from the feasible beam combination set in $\mathcal{A}_l^{\mathsf{FD}}$. Let us consider an HD beam codebook comprised of 8 beams $\mathcal{W}_l^{\mathsf{HD}} = \{\mathbf{w}_{l,1}^{\mathsf{RF}}, \mathbf{w}_{l,2}^{\mathsf{RF}}, \cdots, \mathbf{w}_{l,8}^{\mathsf{RF}}\}$ as an example, where we assume that $\mathbf{v}_l^{\mathsf{RF}}$ is fixed. Assuming that a feasible beam combination set for two UEs satisfying (19) is $\mathcal{A}_l^{\mathsf{FD}} = \{(\mathbf{w}_{l,1}^{\mathsf{RF}}, \mathbf{w}_{l,2}^{\mathsf{RF}}), (\mathbf{w}_{l,3}^{\mathsf{RF}}, \mathbf{w}_{l,4}^{\mathsf{RF}}), (\mathbf{w}_{l,4}^{\mathsf{RF}}, \mathbf{w}_{l,7}^{\mathsf{RF}})\}$. Based on $\mathcal{A}_l^{\mathsf{FD}}$, the new FD codebook can be formed as $\mathcal{W}_l^{\mathsf{FD}} = \{\mathbf{w}_{l,1}^{\mathsf{RF}}, \mathbf{w}_{l,2}^{\mathsf{RF}}, \mathbf{w}_{l,3}^{\mathsf{RF}}, \mathbf{w}_{l,4}^{\mathsf{RF}}, \mathbf{w}_{l,7}^{\mathsf{RF}}\}$.

For an access link transmission, FD SBSs select the beams from $\mathcal{W}_l^{\mathsf{FD}}$, while HD SBSs select the beams from $\mathcal{W}_l^{\mathsf{HD}}$, with $\mathcal{W}_l^{\mathsf{FD}} \subseteq \mathcal{W}_l^{\mathsf{HD}}$. Also, we note that if there are no available beams in $\mathcal{W}_l^{\mathsf{FD}}$, the l-th SBS must operate in HD mode. Based on the above descriptions, we define the transmit RF beam selection constraint at the l-th SBS as follows

$$\begin{cases} \mathbf{w}_{l,k}^{\mathsf{RF}} \in \mathcal{W}_l^{\mathsf{HD}},\ k = 1, 2, \cdots, K & \text{if} \lambda_l = 0\,, \\ (\mathbf{w}_{l,1}^{\mathsf{RF}}, \cdots, \mathbf{w}_{l,K}^{\mathsf{RF}}) \in \mathcal{A}_l^{\mathsf{FD}}, & \text{if} \lambda_l = 1\,. \end{cases} \tag{21}$$

B. System Sum Rate Maximization Problem

In this paper, we aim to maximize the system sum rate by jointly optimizing the BB BF at MBS, $\mathbf{F}^{\mathsf{BB}}$, the transmit BB and RF BF at SBSs, $\mathbf{W}^{\mathsf{BB}} \triangleq \{\mathbf{W}_l^{\mathsf{BB}} | \, l \in \mathcal{L}\}$ and $\mathbf{W}^{\mathsf{RF}} \triangleq \{\mathbf{W}_l^{\mathsf{RF}} | \, l \in \mathcal{L}\}$, and the duplex mode of SBSs, $\boldsymbol{\lambda}$. For the sake of design simplicity, we assume that the RF BF of MBS for transmission and the RF BF of SBSs for the reception in backhaul links are determined by their LoS direction. On the other hand, the RF beams of SBS for transmission in access links are selected from a predefined codebook. Then, the optimization problem can be formulated as

$$\max_{\substack{\boldsymbol{\lambda},\, \mathbf{F}^{\mathsf{BB}} \\ \mathbf{W}^{\mathsf{RF}}, \mathbf{W}^{\mathsf{BB}}}} \ \sum_{l=1}^{L} \min\left\{ R_l^{\mathsf{B}}, \sum_{k=1}^{K} R_{l,k}^{\mathsf{A}} \right\} \tag{22a}$$

$$\text{s.t.} \quad \sum_{l=1}^{L} \left\|\mathbf{f}_l^{\mathsf{BB}}\right\|^2 \leq 1, \tag{22b}$$

$$\sum_{k=1}^{K} \left\|\mathbf{w}_{l,k}^{\mathsf{BB}}\right\|^2 \leq 1,\ \forall l \in \mathcal{L}, \tag{22c}$$

$$\lambda_l \in \{0, 1\},\ \forall l \in \mathcal{L},$$

$$(21). \tag{22d}$$

Constraints (22b) and (22c) represent the transmit power constraints for MBS and each SBS, respectively. Constraint (22d) indicates that the duplex mode variable is binary. This problem is a non-convex mixed integer non-linear programming (MINLP), which is NP-hard and generally difficult to solve, since optimization variables are highly coupled in the objective function and integer variables create non-convex constraints. To overcome this difficulty, we propose an optimization framework which alternately optimizes two

$$\gamma_l^{\mathsf{B},1} = \frac{P_{\mathsf{B}} \left|\mathbf{v}_l^{\mathsf{H}} \mathbf{H}_{0,l} \mathbf{F}^{\mathsf{RF}} \mathbf{f}_l^{\mathsf{BB}}\right|^2}{\sum_{j \neq l}^{L} P_{\mathsf{B}} \left|\mathbf{v}_l^{\mathsf{H}} \mathbf{H}_{0,l} \mathbf{F}^{\mathsf{RF}} \mathbf{f}_j^{\mathsf{BB}}\right|^2 + \sum_{j \neq l}^{L} \sum_{m=1}^{K} \lambda_j P_{\mathsf{A}} \left|\mathbf{v}_l^{\mathsf{H}} \mathbf{H}_{j,l} \mathbf{W}_j^{\mathsf{RF}} \mathbf{w}_{j,m}^{\mathsf{BB}}\right|^2 + \sum_{m=1}^{K} \lambda_l P_{\mathsf{A}} \left\|\mathbf{w}_{l,m}^{\mathsf{BB}}\right\|^2 \sigma_{\mathsf{SI}}^2 + \sigma^2} \tag{12}$$

$$\gamma_l^{\mathsf{B},2} = \frac{\lambda_l P_{\mathsf{B}} \left|\mathbf{v}_l^{\mathsf{H}} \mathbf{H}_{0,l} \mathbf{F}^{\mathsf{RF}} \mathbf{f}_l^{\mathsf{BB}}\right|^2}{\sum_{j \neq l}^{L} \lambda_j P_{\mathsf{B}} \left|\mathbf{v}_l^{\mathsf{H}} \mathbf{H}_{0,l} \mathbf{F}^{\mathsf{RF}} \mathbf{f}_j^{\mathsf{BB}}\right|^2 + \sum_{j \neq l}^{L} \sum_{m=1}^{K} P_{\mathsf{A}} \left|\mathbf{v}_l^{\mathsf{H}} \mathbf{H}_{j,l} \mathbf{W}_j^{\mathsf{RF}} \mathbf{w}_{j,m}^{\mathsf{BB}}\right|^2 + \sum_{m=1}^{K} \lambda_l P_{\mathsf{A}} \left\|\mathbf{w}_{l,m}^{\mathsf{BB}}\right\|^2 \sigma_{\mathsf{SI}}^2 + \sigma^2} \tag{13}$$

$$\gamma_{l,k}^{\mathsf{A},1} = \frac{\lambda_l P_{\mathsf{A}} \left|\mathbf{g}_{l,l,k} \mathbf{W}_l^{\mathsf{RF}} \mathbf{w}_{l,k}^{\mathsf{BB}}\right|^2}{\sum_{j=1}^{L} P_{\mathsf{B}} \left|\mathbf{g}_{0,l,k} \mathbf{F}^{\mathsf{RF}} \mathbf{f}_j^{\mathsf{BB}}\right|^2 + \sum_{j \neq l}^{L} \sum_{m=1}^{K} \lambda_j P_{\mathsf{A}} \left|\mathbf{g}_{j,l,k} \mathbf{W}_j^{\mathsf{RF}} \mathbf{w}_{j,m}^{\mathsf{BB}}\right|^2 + \sum_{m \neq k}^{K} \lambda_l P_{\mathsf{A}} \left|\mathbf{g}_{l,l,k} \mathbf{W}_l^{\mathsf{RF}} \mathbf{w}_{l,m}^{\mathsf{BB}}\right|^2 + \sigma^2} \tag{14}$$

$$\gamma_{l,k}^{\mathsf{A},2} = \frac{P_{\mathsf{A}} \left|\mathbf{g}_{l,l,k} \mathbf{W}_l^{\mathsf{RF}} \mathbf{w}_{l,k}^{\mathsf{BB}}\right|^2}{\sum_{j=1}^{L} \lambda_j P_{\mathsf{B}} \left|\mathbf{g}_{0,l,k} \mathbf{F}^{\mathsf{RF}} \mathbf{f}_j^{\mathsf{BB}}\right|^2 + \sum_{j \neq l}^{L} \sum_{m=1}^{K} P_{\mathsf{A}} \left|\mathbf{g}_{j,l,k} \mathbf{W}_j^{\mathsf{RF}} \mathbf{w}_{j,m}^{\mathsf{BB}}\right|^2 + \sum_{m \neq k}^{K} P_{\mathsf{A}} \left|\mathbf{g}_{l,l,k} \mathbf{W}_l^{\mathsf{RF}} \mathbf{w}_{l,m}^{\mathsf{BB}}\right|^2 + \sigma^2} \tag{15}$$

Authorized licensed use limited to: Univ Of Incheon. Downloaded on October 26,2026 at 13:17:40 UTC from IEEE Xplore. Restrictions apply.

subproblems, namely, hybrid BF design, and duplex mode selection, which are presented in the following sections.

IV. Two-Stage Hybrid Beamforming Design

In this section, we propose a two-stage hybrid BF design algorithm for solving problem (22) with fixed duplex mode. In the first stage, we formulate the RF beam selection subproblem and propose a greedy beam selection procedure to be performed at each SBS. In the second stage, we formulate the BB BF optimization problem with fixed RF BF and approximate a non-smooth minimum function to handle a max-min optimization problem. Then, we derive the first-order Karush-Kuhn-Tucker (KKT) condition for the reformulated BB BF problem, which has the form of a generalized eigenvector problem. To solve this problem, the generalized power iteration (GPI) algorithm is employed to identify the principal eigenvector, which provides the best local optimal solution.

A. Greedy RF Beam Selection

In the first stage, given the duplex mode and the BB BF, each SBS selects multiple RF beams for serving multi-UE from the predetermined HD or FD codebook in (21) according to its duplex mode. The RF beam selection problem can be reformulated as

$$\max_{\mathbf{W}^{\mathsf{RF}}} \sum_{l=1}^{L} \min\left\{R_l^{\mathsf{B}}, \sum_{k=1}^{K} R_{l,k}^{\mathsf{A}}\right\} \tag{23a}$$

$$\text{s.t.} \quad \mathbf{F}^{\mathsf{BB}} = \frac{1}{\sqrt{L}}\mathbf{I}_L, \mathbf{W}_l^{\mathsf{BB}} = \frac{1}{\sqrt{K}}\mathbf{I}_K, \ \forall l \in \mathcal{L}, \quad (21). \tag{23b}$$

Here, equal power allocation is assumed for the RF beam selection procedure. Since the transmit RF beams of all the SBSs are strongly coupled to each other as in (12)-(15), it is challenging to design an efficient algorithm for problem (23). Although an exhaustive search over all possible beam combinations will give the optimal solution of problem (23), this incurs prohibitively high complexity and is infeasible in a practical system.

To make the problem (23) tractable in order to design an efficient algorithm, we optimize the lower-bound of the objective function (23a). By restricting the power of ISI and ICI which result from other SBS to the l-th SBSs below threshold values δ_l and $\delta_{l,k}$, respectively, a lower-bound of the objective function (23a) can be written as

$$\begin{aligned} R_{\mathsf{lb}} &= \sum_{l=1}^{L} 0.5 \cdot \min\left\{ \log_2\left(1+\frac{\hat{h}_{l,l}}{I_l^{\mathsf{B},1}}\right) + \log_2\left(1+\frac{\lambda_l \hat{h}_{l,l}}{I_l^{\mathsf{B},2}}\right), \right. \\ &\sum_{k=1}^{K}\left(\log_2\left(1+\frac{\lambda_l P_{\mathsf{A}}|\mathbf{g}_{l,l,k}\mathbf{w}_{l,k}^{\mathsf{RF}}|^2}{I_{l,k}^{\mathsf{A},1}+\sum_{m\neq k}^{K}\lambda_l P_{\mathsf{A}}|\mathbf{g}_{l,l,k}\mathbf{w}_{l,m}^{\mathsf{RF}}|^2}\right)\right. \\ &\left.\left.+\log_2\left(1+\frac{P_{\mathsf{A}}|\mathbf{g}_{l,l,k}\mathbf{w}_{l,k}^{\mathsf{RF}}|^2}{I_{l,k}^{\mathsf{A},2}+\sum_{m\neq k}^{K}P_{\mathsf{A}}|\mathbf{g}_{l,l,k}\mathbf{w}_{l,m}^{\mathsf{RF}}|^2}\right)\right)\right\}, \end{aligned} \tag{24}$$

where

$$\begin{aligned} I_l^{\mathsf{B},1} &= \sum_{j\neq l}^{L}\left(\frac{P_{\mathsf{B}}}{L}|\mathbf{v}_l^{\mathsf{H}}\mathbf{H}_{0,l}\mathbf{f}_j^{\mathsf{RF}}|^2 + \lambda_j K\delta_l\right) + \lambda_l P_{\mathsf{A}}\sigma_{\mathsf{SI}}^2 + \sigma^2 \\ I_l^{\mathsf{B},2} &= \sum_{j\neq l}^{L}\left(\frac{P_{\mathsf{B}}}{L}\lambda_j|\mathbf{v}_l^{\mathsf{H}}\mathbf{H}_{0,l}\mathbf{f}_j^{\mathsf{RF}}|^2 + K\delta_l\right) + \lambda_l P_{\mathsf{A}}\sigma_{\mathsf{SI}}^2 + \sigma^2 \\ I_{l,k}^{\mathsf{A},1} &= \sum_{j=1}^{L}\frac{P_{\mathsf{B}}}{L}|\mathbf{g}_{0,l,k}\mathbf{f}_j^{\mathsf{RF}}|^2 + \sum_{j\neq l}^{L}\lambda_j K\delta_{l,k} + \sigma^2 \\ I_{l,k}^{\mathsf{A},2} &= \sum_{j=1}^{L}\frac{P_{\mathsf{B}}}{L}\lambda_j|\mathbf{g}_{0,l,k}\mathbf{f}_j^{\mathsf{RF}}|^2 + \sum_{j\neq l}^{L}K\delta_{l,k} + \sigma^2 \\ \hat{h}_{l,l} &= \frac{P_{\mathsf{B}}}{L}|\mathbf{v}_l^{\mathsf{H}}\mathbf{H}_{0,l}\mathbf{f}_l^{\mathsf{RF}}|^2 \end{aligned} \tag{25}$$

Note that, in (24), the backhaul data rate is not affected by the RF beams $\mathbf{W}^{\mathsf{RF}}$, and the access data rate of each SBS is solely determined by its transmit beams. Therefore, we can divide the problem (23) into L subproblems and each subproblem is to maximize the access link data rate of the l-th SBS given by

$$\max_{\mathbf{W}_l^{\mathsf{RF}}} \sum_{k=1}^{K}\log_2\left(1+\frac{P_{\mathsf{A}}|\mathbf{g}_{l,l,k}\mathbf{w}_{l,k}^{\mathsf{RF}}|^2}{I_{l,k}^{\mathsf{A},2}+\sum_{m\neq k}^{K}P_{\mathsf{A}}|\mathbf{g}_{l,l,k}\mathbf{w}_{j,m}^{\mathsf{RF}}|^2}\right) \tag{26a}$$

$$\text{s.t.} \quad \frac{P_{\mathsf{A}}}{K}|\mathbf{v}^{\mathsf{H}}\mathbf{H}_{j,l}\mathbf{w}_{j,m}^{\mathsf{RF}}|^2 \leq \delta_l, \frac{P_{\mathsf{A}}}{K}|\mathbf{g}_{j,l,k}\mathbf{w}_{j,m}^{\mathsf{RF}}|^2 \leq \delta_{l,k}, \ \forall l, j \in \mathcal{L}, j \neq l, \quad (21). \tag{26b}$$

where (26b) is the RF beam constraint for restricting ISI and ICI power levels. Then, we can re-define the HD codebook, the FD beam combination set, and the FD codebook as $\mathcal{W}_{l,\mathsf{lb}}^{\mathsf{HD}}$, $\mathcal{A}_{l,\mathsf{lb}}^{\mathsf{FD}}$, and $\mathcal{W}_{l,\mathsf{lb}}^{\mathsf{FD}}$, respectively, satisfying the constraints (21) and (26b).

Solving problem (26) using an exhaustive search still requires prohibitive complexity in order of $\mathcal{O}(|\mathcal{W}|!)$. Furthermore, for each FD SBS cell, there is an additional constraint considering not only the FD codebook $\mathcal{W}_{l,\mathsf{lb}}^{\mathsf{FD}}$ but also the beam combination set $\mathcal{A}_{l,\mathsf{lb}}^{\mathsf{FD}}$. To deal with this difficulty, we propose a greedy beam assignment algorithm with low complexity, which finds the best UE-beam combination in a greedy manner to maximize the objective value. The detailed procedure of the proposed algorithm is described as follows.

1) We first initialize the set of UE-beam combination at the l-th SBS as $\Omega_l = \emptyset$, $\forall l$. The l-th SBS constructs the matrix $\mathbf{R}_l^z$ using beams in the codebook, depending on the duplex mode $z \in \{\mathsf{HD}, \mathsf{FD}\}$, as follows

$$\mathbf{R}_l^z = [\mathbf{r}_{l,1}^z|\cdots|\mathbf{r}_{l,|\mathcal{W}_{l,\mathsf{lb}}^z|}^z] \in \mathbb{R}_+^{K\times|\mathcal{W}_{l,\mathsf{lb}}^z|}, \tag{27}$$

where $\mathbf{r}_{l,m}^z$ is constructed by the beam domain channel gain from the m-th beam of each codebook, denoted as $\mathbf{w}_m^{\mathsf{RF},z}$, to all UEs, as follows

$$\mathbf{r}_{l,m}^z = [f_{l,1}(|\mathbf{g}_{l,l,1}\mathbf{w}_{l,m}^{\mathsf{RF},z}|^2), \cdots, f_{l,K}(|\mathbf{g}_{l,l,K}\mathbf{w}_{l,m}^{\mathsf{RF},z}|^2)]^{\mathsf{T}}, \tag{28}$$

with $f_{l,k}(x) \triangleq \log_2\left(1+\frac{P_{\mathsf{A}}x}{I_{l,k}^{\mathsf{A},2}}\right)$.

Authorized licensed use limited to: Univ Of Incheon. Downloaded on October 26,2026 at 13:17:40 UTC from IEEE Xplore. Restrictions apply.

2) The best UE-beam combination is selected from the row-column index pair with the largest element in $\mathbf{R}_l^z$ as follows

$$(u^*, b^*) = \arg\max_{u,b} \left\{ [\mathbf{R}_l^z]_{u,b} \right\}. \quad (29)$$

3) The set of UE-beam combination is updated as follows

$$\Omega_l = \Omega_l \cup \{(u^*, b^*)\}, \quad (30)$$

After updating Ω_l, we set the elements of u^*-th row and the b^*-th column in $\mathbf{R}_l^z$ to zero. In addition, when the l-th SBS is operating in FD, we need to find the beam combination from $\mathcal{A}_{l,\mathsf{lb}}^{\mathsf{FD}}$, which does not include $\mathbf{w}_{b^*}^{\mathsf{RF},z}$ as an element, and define the set of beam indices in the obtained beam combinations as $\mathcal{I}_{l,b^*}$. Then, we set the elements of columns whose indices are included in $\mathcal{I}_{l,b^*}$ to zero. We also update the interference of UEs by adding interference caused by the b^*-th beam as

$$I_{l,k}^{\mathsf{A},2} = I_{l,k}^{\mathsf{A},2} + P_{\mathsf{A}} |\mathbf{g}_{l,l,k} \mathbf{w}_{l,b^*}^{\mathsf{RF},z}|^2, \; k = 1, \cdots, K. \quad (31)$$

Then, we reconstruct $\mathbf{R}_l^z$ for non-zero values as in (27).

4) Repeat the procedures in 2) and 3) until K UE-beam combinations are formed.

Algorithm 1 Greedy RF Beam Selection Algorithm

Require: $\boldsymbol{\lambda}, \mathcal{W}_{l,\mathsf{lb}}^{\mathsf{HD}}, \mathcal{W}_{l,\mathsf{lb}}^{\mathsf{FD}}, \mathcal{A}_{l,\mathsf{lb}}^{\mathsf{FD}}, \forall l \in \mathcal{L}$
Set $\mathbf{F}^{\mathsf{BB}} = \frac{1}{\sqrt{L}} \mathbf{I}_L, \mathbf{W}_l^{\mathsf{BB}} = \frac{1}{\sqrt{K}} \mathbf{I}_K, \forall l \in \mathcal{L}$
Initialize $\Omega_l = \emptyset, \mathbf{W}_l^{\mathsf{RF}} = \text{Empty Matrix}, \forall l \in \mathcal{L}$
for $l = 1 : L$ **do**
  if $\lambda_l = 0$ **then**
    $z = \mathsf{HD}$
  else
    $z = \mathsf{FD}$
  end if
  Construct $\mathbf{R}_l^z$ as in (27)
  while $|\Omega_l| < K$ **do**
    $(u^*, b^*) \leftarrow \arg\max_{u,b} \left\{ [\mathbf{R}_l^z]_{u,b} \right\}$
    $\Omega_l \leftarrow \Omega_l \cup (u^*, b^*)$
    $\mathbf{W}_l^{\mathsf{RF}} \leftarrow [\mathbf{W}_l^{\mathsf{RF}} | \mathbf{w}_{b^*}^{\mathsf{RF},z}]$
    Set the elements of u^*th row and b^*th column in $\mathbf{R}_l^z$ to zero
    if $z = \mathsf{FD}$ **then**
      Find $\mathcal{I}_{l,b^*}$
      for $i \in \mathcal{I}_{l,b^*}$ **do**
        Set the elements of ith column in $\mathbf{R}_l^z$ to zero
      end for
    end if
    Update $I_{l,k}^{\mathsf{A},2}, \forall k = 1, \cdots, K$ as in (31)
    Reconstruct $\mathbf{R}_l^z$ for non-zero values as in (27)
  end while
end for
return: $\mathbf{W}_l^{\mathsf{RF}}, \forall l \in \mathcal{L}$

From the above algorithm, each $\mathbf{W}_l^{\mathsf{RF}}$ is composed of the selected beams in Ω_l. At each iteration, each SBS independently finds the best UE-beam combination for maximizing the lower bound of achievable rate with an update of the interference caused by selected UE-beam combinations at the previous iteration. Thus, the proposed greedy RF beam selection algorithm can ensure minimum performance of UEs with a lower complexity compared to an exhaustive search. The overall proposed RF beam selection algorithm is summarized in Algorithm 1.

B. Baseband Beamforming Optimization With Generalized Power Iteration

With the obtained RF BF and fixed duplex mode, the sub-problem of (22) for the BB BF design can be formulated as

$$\max_{\mathbf{F}^{\mathsf{BB}}, \mathbf{W}^{\mathsf{BB}}} \; \sum_{l=1}^{L} \min \left\{ R_l^{\mathsf{B}}, \sum_{k=1}^{K} R_{l,k}^{\mathsf{A}} \right\} \quad (32a)$$

$$\text{s.t.} \; \sum_{l=1}^{L} \|\mathbf{f}_l^{\mathsf{BB}}\|^2 \le 1, \quad (32b)$$

$$\sum_{k=1}^{K} \|\mathbf{w}_{l,k}^{\mathsf{BB}}\|^2 \le 1, \; \forall l \in \mathcal{L}. \quad (32c)$$

However, it is still difficult to solve (32) due to the non-convex objective function. To transform the objective function into a tractable form, we define a higher-dimensional vector by concatenating all BB BF vectors of the MBS $\mathbf{f}_l^{\mathsf{BB}}$, and SBS $\mathbf{w}_{l,m}^{\mathsf{BB}}$, as

$$\mathbf{q} = [\mathbf{f}_1^{\mathsf{BB}\,\mathsf{H}}, \cdots, \mathbf{f}_L^{\mathsf{BB}\,\mathsf{H}}, \mathbf{w}_{1,1}^{\mathsf{BB}\,\mathsf{H}}, \cdots, \mathbf{w}_{L,K}^{\mathsf{BB}\,\mathsf{H}}]^{\mathsf{H}} \in \mathbb{C}^{(L^2+LK^2)\times 1}. \quad (33)$$

Based on (33), we can express the backhaul link data rates of the l-th SBS at each time slot $R_l^{\mathsf{B},1}$ and $R_l^{\mathsf{B},2}$

$$R_l^{\mathsf{B},1} = \log_2 \left(\frac{\mathbf{q}^{\mathsf{H}} \mathbf{A}_l^1 \mathbf{q}}{\mathbf{q}^{\mathsf{H}} \mathbf{B}_l^1 \mathbf{q}} \right), \; R_l^{\mathsf{B},2} = \log_2 \left(\frac{\mathbf{q}^{\mathsf{H}} \mathbf{A}_l^2 \mathbf{q}}{\mathbf{q}^{\mathsf{H}} \mathbf{B}_l^2 \mathbf{q}} \right). \quad (34)$$

where $\mathbf{A}_l^1$, $\mathbf{A}_l^2$, $\mathbf{B}_l^1$, and $\mathbf{B}_l^2$ are defined as

$$\begin{aligned}
\mathbf{A}_l^1 =& \,\mathsf{blkdiag} \Big(\mathbf{I}_L \otimes \tilde{\mathbf{h}}_{0,l}^{\mathsf{H}} \tilde{\mathbf{h}}_{0,l}, \lambda_1 \frac{P_{\mathsf{A}}}{P_{\mathsf{B}}} \mathbf{I}_K \otimes \tilde{\mathbf{h}}_{1,l}^{\mathsf{H}} \tilde{\mathbf{h}}_{1,l}, \\
& \cdots, \lambda_l \frac{P_{\mathsf{A}} \sigma_{\mathsf{SI}}^2}{P_{\mathsf{B}}} \mathbf{I}_{K^2}, \cdots, \lambda_L \frac{P_{\mathsf{A}}}{P_{\mathsf{B}}} \mathbf{I}_K \otimes \tilde{\mathbf{h}}_{L,l}^{\mathsf{H}} \tilde{\mathbf{h}}_{L,l} \Big) \\
& + \frac{\sigma^2}{P_{\mathsf{B}}(L+1)} \mathbf{I}_{(L^2+LK^2)}, \\
\mathbf{B}_l^1 =& \, \mathbf{A}_l^1 - \mathsf{blkdiag} \left(\mathbf{e}_l \mathbf{e}_l^{\mathsf{T}} \otimes \tilde{\mathbf{h}}_{0,l}^{\mathsf{H}} \tilde{\mathbf{h}}_{0,l}, \mathbf{0}_{LK^2} \right) \\
\mathbf{A}_l^2 =& \,\mathsf{blkdiag} \Big(\mathsf{diag}(\boldsymbol{\lambda}) \otimes \tilde{\mathbf{h}}_{0,l}^{\mathsf{H}} \tilde{\mathbf{h}}_{0,l}, \frac{P_{\mathsf{A}}}{P_{\mathsf{B}}} \mathbf{I}_K \otimes \tilde{\mathbf{h}}_{1,l}^{\mathsf{H}} \tilde{\mathbf{h}}_{1,l}, \\
& \cdots, \lambda_l \frac{P_{\mathsf{A}} \sigma_{\mathsf{SI}}^2}{P_{\mathsf{B}}} \mathbf{I}_{K^2}, \cdots, \frac{P_{\mathsf{A}}}{P_{\mathsf{B}}} \mathbf{I}_K \otimes \tilde{\mathbf{h}}_{L,l}^{\mathsf{H}} \tilde{\mathbf{h}}_{L,l} \Big) \\
& + \frac{\sigma^2}{P_{\mathsf{B}}(L+1)} \mathbf{I}_{(L^2+LK^2)}, \\
\mathbf{B}_l^2 =& \, \mathbf{A}_l^2 - \mathsf{blkdiag} \left(\lambda_l \mathbf{e}_l \mathbf{e}_l^{\mathsf{T}} \otimes \tilde{\mathbf{h}}_{0,l}^{\mathsf{H}} \tilde{\mathbf{h}}_{0,l}, \mathbf{0}_{LK^2} \right).
\end{aligned} \quad (35)$$

Here $\tilde{\mathbf{h}}_{0,l} = \mathbf{v}_l^{\mathsf{H}} \mathbf{H}_{0,l} \mathbf{F}^{\mathsf{RF}}$, $\tilde{\mathbf{h}}_{j,l} = \mathbf{v}_l^{\mathsf{H}} \mathbf{H}_{j,l} \mathbf{W}_j^{\mathsf{RF}}$, $\tilde{\mathbf{g}}_{0,l,k} = \mathbf{g}_{0,l,k} \mathbf{F}^{\mathsf{RF}}$ and $\tilde{\mathbf{g}}_{j,l,k} = \mathbf{g}_{j,l,k} \mathbf{W}_j^{\mathsf{RF}}$ are denoted as effective RF beam domain channels for all links. Similarly, we can rewrite

Authorized licensed use limited to: Univ Of Incheon. Downloaded on October 26,2026 at 13:17:40 UTC from IEEE Xplore. Restrictions apply.

the access link data rates of the k-th UE served by the l-th SBS at each time slot $R_{l,k}^{\mathsf{A},1}$ and $R_{l,k}^{\mathsf{A},2}$ as

$$R_{l,k}^{\mathsf{A},1} = \log_2\left(\frac{\mathbf{q}^{\mathsf{H}}\mathbf{C}_{l,k}^1\mathbf{q}}{\mathbf{q}^{\mathsf{H}}\mathbf{D}_{l,k}^1\mathbf{q}}\right),\ R_{l,k}^{\mathsf{A},2} = \log_2\left(\frac{\mathbf{q}^{\mathsf{H}}\mathbf{C}_{l,k}^2\mathbf{q}}{\mathbf{q}^{\mathsf{H}}\mathbf{D}_{l,k}^2\mathbf{q}}\right), \quad (36)$$

where $\mathbf{C}_{l,k}^1$, $\mathbf{C}_{l,k}^2$, $\mathbf{D}_{l,k}^1$, and $\mathbf{D}_{l,k}^2$ are defined as

$$\begin{aligned}
&\mathbf{C}_{l,k}^1 \\
&= \mathsf{blkdiag}\left(\mathbf{I}_L \otimes \tilde{\mathbf{g}}_{0,l,k}^{\mathsf{H}}\tilde{\mathbf{g}}_{0,l,k}, \lambda_1\frac{P_{\mathsf{A}}}{P_{\mathsf{B}}}\mathbf{I}_K \otimes \tilde{\mathbf{g}}_{1,l,k}^{\mathsf{H}}\tilde{\mathbf{g}}_{1,l,k},\right. \\
&\quad \left.\cdots, \lambda_L\frac{P_{\mathsf{A}}}{P_{\mathsf{B}}}\mathbf{I}_K \otimes \tilde{\mathbf{g}}_{L,l,k}^{\mathsf{H}}\tilde{\mathbf{g}}_{L,l,k}\right) + \frac{\sigma^2}{P_{\mathsf{B}}(L+1)}\mathbf{I}_{(L^2+LK^2)}, \\
&\mathbf{D}_{l,k}^1 \\
&= \mathbf{C}_{l,k}^1 - \mathsf{blkdiag}\left(\mathbf{0}_{L^2}, \lambda_l\frac{P_{\mathsf{A}}}{P_{\mathsf{B}}}\mathbf{e}_{l_k}\mathbf{e}_{l_k}^{\mathsf{T}} \otimes \tilde{\mathbf{g}}_{l,l,k}^{\mathsf{H}}\tilde{\mathbf{g}}_{l,l,k}\right), \\
&\mathbf{C}_{l,k}^2 \\
&= \mathsf{blkdiag}\left(\mathsf{diag}(\boldsymbol{\lambda}) \otimes \tilde{\mathbf{g}}_{0,l,k}^{\mathsf{H}}\tilde{\mathbf{g}}_{0,l,k}, \frac{P_{\mathsf{A}}}{P_{\mathsf{B}}}\mathbf{I}_K \otimes \tilde{\mathbf{g}}_{1,l,k}^{\mathsf{H}}\tilde{\mathbf{g}}_{1,l,k},\right. \\
&\quad \left.\cdots, \frac{P_{\mathsf{A}}}{P_{\mathsf{B}}}\mathbf{I}_K \otimes \tilde{\mathbf{g}}_{L,l,k}^{\mathsf{H}}\tilde{\mathbf{g}}_{L,l,k}\right) + \frac{\sigma^2}{P_{\mathsf{B}}(L+1)}\mathbf{I}_{(L^2+LK^2)}, \\
&\mathbf{D}_{l,k}^2 \\
&= \mathbf{C}_{l,k}^2 - \mathsf{blkdiag}\left(\mathbf{0}_{L^2}, \frac{P_{\mathsf{A}}}{P_{\mathsf{B}}}\mathbf{e}_{l_k}\mathbf{e}_{l_k}^{\mathsf{T}} \otimes \tilde{\mathbf{g}}_{l,l,k}^{\mathsf{H}}\tilde{\mathbf{g}}_{l,l,k}\right). \quad (37)
\end{aligned}$$

with $l_k = L^2 + K(l-1) + k$.

Based on (34) and (36), the system sum rate (18) can be rewritten as

$$R^{\mathsf{sum}} = 0.5 \cdot \sum_{l=1}^{L} \min\left\{\log_2\left(\frac{\mathbf{q}^{\mathsf{H}}\mathbf{A}_l^1\mathbf{q}}{\mathbf{q}^{\mathsf{H}}\mathbf{B}_l^1\mathbf{q}}\right)\left(\frac{\mathbf{q}^{\mathsf{H}}\mathbf{A}_l^2\mathbf{q}}{\mathbf{q}^{\mathsf{H}}\mathbf{B}_l^2\mathbf{q}}\right), \log_2\prod_{k=1}^{K}\left(\frac{\mathbf{q}^{\mathsf{H}}\mathbf{C}_{l,k}^1\mathbf{q}}{\mathbf{q}^{\mathsf{H}}\mathbf{D}_{l,k}^1\mathbf{q}}\right)\left(\frac{\mathbf{q}^{\mathsf{H}}\mathbf{C}_{l,k}^2\mathbf{q}}{\mathbf{q}^{\mathsf{H}}\mathbf{D}_{l,k}^2\mathbf{q}}\right)\right\}. \quad (38)$$

We note that the sum rate in (38) is expressed as the sum of non-smooth minimum function, which is still intractable. Thus, we employ the LogSumExp technique to approximate the minimum function as [42]

$$\min_{n=1,\cdots,N}\{x_n\} \approx -\alpha \ln\left(\sum_{n=1}^{N}\exp\left(-\frac{1}{\alpha}x_n\right)\right), \quad (39)$$

Note that this approximation becomes tight as $\alpha \to 0$. Then, the system sum rate R^{sum} can be approximated by a smooth differentiable function as

$$\begin{aligned}
R^{\mathsf{sum}} \approx 0.5 \cdot \sum_{l=1}^{L} -\alpha_l \ln\left(\left(\frac{\mathbf{q}^{\mathsf{H}}\mathbf{A}_l^1\mathbf{q}\,\mathbf{q}^{\mathsf{H}}\mathbf{A}_l^2\mathbf{q}}{\mathbf{q}^{\mathsf{H}}\mathbf{B}_l^1\mathbf{q}\,\mathbf{q}^{\mathsf{H}}\mathbf{B}_l^2\mathbf{q}}\right)^{\beta_l}\right. \\
\left. + \prod_{k=1}^{K}\left(\frac{\mathbf{q}^{\mathsf{H}}\mathbf{C}_{l,k}^1\mathbf{q}\,\mathbf{q}^{\mathsf{H}}\mathbf{C}_{l,k}^2\mathbf{q}}{\mathbf{q}^{\mathsf{H}}\mathbf{D}_{l,k}^1\mathbf{q}\,\mathbf{q}^{\mathsf{H}}\mathbf{D}_{l,k}^2\mathbf{q}}\right)^{\beta_l}\right) \triangleq \delta(\mathbf{q}). \quad (40)
\end{aligned}$$

where $\beta_l = -\frac{1}{\alpha_l \ln 2}$. We can reformulate the problem (32) based on (33) and (40) as

$$\begin{aligned}
&\max_{\mathbf{q}} \quad \delta(\mathbf{q}) \quad (41)\\
&\text{s.t.} \quad \text{(32b), (32c).}
\end{aligned}$$

Note that the transmit power constraints of MBS and SBSs incur significant challenges in solving the problem. To make the problem (41) in a more tractable form, we relax the power constraints of MBS and SBSs to a sum-power constraint with respect to $\mathbf{q}$, i.e., $\|\mathbf{q}\|^2 \le L+1$, and then we aim to find a local optimal solution satisfying the first-order KKT condition of problem (41). It is worth noting that $\delta(\mathbf{q}) = \delta(\kappa\mathbf{q})$ and $\frac{\partial\delta(\mathbf{q})}{\partial\mathbf{q}} = \kappa\frac{\partial\delta(\kappa\mathbf{q})}{\partial\mathbf{q}}$ holds for any nonzero κ [43]. Therefore, if $\mathbf{q}^\star$ is a local optimal solution that satisfies the first-order KKT conditions of the problem (41) without the sum power constraint, then $\kappa\mathbf{q}^\star$ is also a local optimal solution satisfying the same first-order KKT conditions due to $\delta(\mathbf{q}^\star) = \delta(\kappa\mathbf{q}^\star)$. In other words, after obtaining $\mathbf{q}^\star$ satisfying the first-order KKT condition of the problem (41) while ignoring the sum power constraint, we can obtain a local optimal solution satisfying the sum power constraint by normalizing $\mathbf{q}^\star$ to satisfy $\|\mathbf{q}^\star\|^2 \le L+1$. Therefore, in the following Lemma, we derive the first-order KKT condition of the problem (41) without the power constraints.

Lemma 1: The first-order KKT optimality condition of the optimization problem (41) can be derived as

$$\mathbf{X}_{\mathsf{KKT}}(\mathbf{q})\mathbf{q} = \delta(\mathbf{q})\mathbf{Y}_{\mathsf{KKT}}(\mathbf{q})\mathbf{q}, \quad (42)$$

where

$$\begin{aligned}
&\mathbf{X}_{\mathsf{KKT}}(\mathbf{q}) \\
&= \delta_{\mathsf{num}}(\mathbf{q})\sum_{l=1}^{L}\beta_l u_l(\mathbf{q})\left(m_l(\mathbf{q})\left(\frac{\mathbf{A}_l^1}{\mathbf{q}^{\mathsf{H}}\mathbf{A}_l^1\mathbf{q}} + \frac{\mathbf{A}_l^2}{\mathbf{q}^{\mathsf{H}}\mathbf{A}_l^2\mathbf{q}}\right)\right. \\
&\quad \left. + n_l(\mathbf{q})\sum_{k=1}^{K}\left(\frac{\mathbf{C}_{l,k}^1}{\mathbf{q}^{\mathsf{H}}\mathbf{C}_{l,k}^1\mathbf{q}} + \frac{\mathbf{C}_{l,k}^2}{\mathbf{q}^{\mathsf{H}}\mathbf{C}_{l,k}^2\mathbf{q}}\right)\right), \\
&\mathbf{Y}_{\mathsf{KKT}}(\mathbf{q}) \\
&= \delta_{\mathsf{den}}(\mathbf{q})\sum_{l=1}^{L}\beta_l u_l(\mathbf{q})\left(m_l(\mathbf{q})\left(\frac{\mathbf{B}_l^1}{\mathbf{q}^{\mathsf{H}}\mathbf{B}_l^1\mathbf{q}} + \frac{\mathbf{B}_l^2}{\mathbf{q}^{\mathsf{H}}\mathbf{B}_l^1\mathbf{q}}\right)\right. \\
&\quad \left. + n_l(\mathbf{q})\sum_{k=1}^{K}\left(\frac{\mathbf{D}_{l,k}^1}{\mathbf{q}^{\mathsf{H}}\mathbf{D}_{l,k}^1\mathbf{q}} + \frac{\mathbf{D}_{l,k}^2}{\mathbf{q}^{\mathsf{H}}\mathbf{D}_{l,k}^2\mathbf{q}}\right)\right), \\
&m_l(\mathbf{q}) \\
&= \left(\frac{\mathbf{q}^{\mathsf{H}}\mathbf{A}_l^1\mathbf{q}\,\mathbf{q}^{\mathsf{H}}\mathbf{A}_l^2\mathbf{q}}{\mathbf{q}^{\mathsf{H}}\mathbf{B}_l^1\mathbf{q}\,\mathbf{q}^{\mathsf{H}}\mathbf{B}_l^2\mathbf{q}}\right)^{\beta_l}, \\
&n_l(\mathbf{q}) \\
&= \prod_{k=1}^{K}\left(\frac{\mathbf{q}^{\mathsf{H}}\mathbf{C}_{l,k}^1\mathbf{q}\,\mathbf{q}^{\mathsf{H}}\mathbf{C}_{l,k}^2\mathbf{q}}{\mathbf{q}^{\mathsf{H}}\mathbf{D}_{l,k}^1\mathbf{q}\,\mathbf{q}^{\mathsf{H}}\mathbf{D}_{l,k}^2\mathbf{q}}\right)^{\beta_l}, \\
&u_l(\mathbf{q}) \\
&= \frac{\alpha_l}{m_l(\mathbf{q}) + n_l(\mathbf{q})},\ \delta(\mathbf{q}) = \delta_{\mathsf{num}}(\mathbf{q})/\delta_{\mathsf{den}}(\mathbf{q}) \quad (43)
\end{aligned}$$

Proof: See Appendix.□

If the BB BF vector $\mathbf{q}$ satisfies the first-order optimality condition (42), it is a stationary point of (41a), but there may be multiple points satisfying this condition. Thus, our aim is to find the best local optimal point that maximizes the objective function (41a) among these points. We note that (42) can be regarded as a generalized eigenvalue problem. If condition (42) is satisfied, $\mathbf{q}$ becomes an eigenvector of the

Authorized licensed use limited to: Univ Of Incheon. Downloaded on October 26,2026 at 13:17:40 UTC from IEEE Xplore. Restrictions apply.

matrix $\mathbf{Y}_{\mathsf{KKT}}(\mathbf{q})^{-1}\mathbf{X}_{\mathsf{KKT}}(\mathbf{q})$, and $\delta(\mathbf{q})$ is the corresponding eigenvalue. Since $\delta(\mathbf{q})$ serves as the objective function in (41), the principal eigenvector of $\mathbf{Y}_{\mathsf{KKT}}^{-1}\mathbf{X}_{\mathsf{KKT}}$ corresponding to the largest eigenvalue guarantees the best local optimal point among the stationary points in (41).

Note that finding the principal eigenvector is a non-trival task because $\mathbf{Y}_{\mathsf{KKT}}(\mathbf{q})^{-1}\mathbf{X}_{\mathsf{KKT}}(\mathbf{q})$ is dependent on $\mathbf{q}$. To address this difficulty, we adopt a novel algorithm based on generalized power iteration (GPI) approach in [43], which is presented as follows. At each iteration t, we construct the matrices $\mathbf{X}_{\mathsf{KKT}}(\mathbf{q}^{(t)})$ and $\mathbf{Y}_{\mathsf{KKT}}(\mathbf{q}^{(t)})$, and subsequently, the BB BF vector for the next iteration is updated as follows

$$\mathbf{q}^{(t+1)} \leftarrow \frac{\mathbf{Y}_{\mathsf{KKT}}^{-1}(\mathbf{q}^{(t)})\mathbf{X}_{\mathsf{KKT}}(\mathbf{q}^{(t)})\mathbf{q}^{(t)}}{\|\mathbf{Y}_{\mathsf{KKT}}^{-1}(\mathbf{q}^{(t)})\mathbf{X}_{\mathsf{KKT}}(\mathbf{q}^{(t)})\mathbf{q}^{(t)}\|}, \tag{44}$$

This procedure continues until convergence.

Remark 1: Due to the relaxation in (41b), this algorithm does not directly consider the individual power constraints of the MBS and SBSs in the problem (32). To address this issue, the algorithm normalizes the BB BF vector $\mathbf{q}^{(t)}$ obtained in the above iteration process as follows

$$\mathbf{q}^{\star} = \frac{\mathbf{q}^{(t)}}{\max\left\{\sum_{l=1}^{L}\left\|\mathbf{f}_l^{\mathsf{BB}(t)}\right\|^2, \max_{l\in\mathcal{L}}\left\{\sum_{k=1}^{K}\left\|\mathbf{w}_{l,k}^{\mathsf{BB}(t)}\right\|^2\right\}\right\}}. \tag{45}$$

By applying this normalization, the obtained BB BF vector $\mathbf{q}^{\star}$ satisfies the power constraints (32b) and (32c) for the MBS and SBSs, respectively.

Algorithm 2 GPI Based Baseband Beamforming Optimization Algorithm

Require: $\boldsymbol{\lambda}, \mathbf{F}^{\mathsf{RF}}, \mathbf{W}_l^{\mathsf{RF}}, \forall l \in \mathcal{L}$
Set the iteration count $t = 0$
Initialize $\mathbf{q}_{(0)} = \mathsf{MRT}$
while $\|\mathbf{q}^{(t)} - \mathbf{q}^{(t-1)}\| > \epsilon$ and $t \le t_{\max}$ **do**
Construct the matrices $\mathbf{X}_{\mathsf{KKT}}(\mathbf{q}^{(t)})$ and $\mathbf{Y}^{\mathsf{KKT}}(\mathbf{q}_{(t)})$
Update $\mathbf{q}^{(t+1)} \leftarrow \frac{\mathbf{Y}_{\mathsf{KKT}}^{-1}(\mathbf{q}^{(t)})\mathbf{X}_{\mathsf{KKT}}(\mathbf{q}^{(t)})\mathbf{q}^{(t)}}{\|\mathbf{Y}_{\mathsf{KKT}}^{-1}(\mathbf{q}^{(t)})\mathbf{X}_{\mathsf{KKT}}(\mathbf{q}^{(t)})\mathbf{q}^{(t)}\|}$
Set $t \leftarrow t+1$
end while
Obtain $\mathbf{q}^{\star}$ by normalizing $\mathbf{q}^{(t)}$ as in (45)
return: $\mathbf{F}^{\mathsf{BB}}$,$\mathbf{W}_l^{\mathsf{BB}}$, $\forall l \in \mathcal{L}$

Based on $\mathbf{q}^{\star}$, we finally obtain $\mathbf{F}^{\mathsf{BB}}$ and $\mathbf{W}^{\mathsf{BB}}$ as in (33). The detailed descriptions of our proposed BB BF design algorithm is presented in Algorithm 2.

V. Worst Mode Switching (WMS) Algorithm

In this section, we optimize the duplex modes of SBSs $\boldsymbol{\lambda}$ to maximize the system sum rate in (22). An exhaustive search can be employed to find the optimal duplex modes, but incurs an exponential complexity of $\mathcal{O}(2^L)$. Therefore, we propose a novel iterative duplex mode selection algorithm which converges to a near-optimal solution in a polynomial time. We adopt the idea of worst case switching in [44] but adapt the switching steps specifically to the problem at hand. We note the following two rationales: 1) The HD SBS cell with the worst data rate does not utilize full-time resources, and 2) The FD SBS cell with the worst data rate is significantly affected by additional interference from other SBSs and the available set of SBS transmit beams is limited by (19). In other words, switching the HD mode of the worst SBS cell to the FD mode is likely to use full-time resource, while switching the FD mode of the worst SBS to the HD mode is likely to suppress interference and utilize more SBS transmit beams. As a result, the proposed algorithm is designed to switch the mode of the worst SBS, leading to a higher system sum rate. We describe this algorithm in the following subsections, and will verify its near-optimal performance by comparing with an exhaustive search solution in section vi.

A. Algorithm Description

We first denote $R_l(\boldsymbol{\lambda}^{(t)})$ and $R^{\mathsf{sum}}(\boldsymbol{\lambda}^{(t)})$ as the end-to-end rate of the l-th SBS cell and the system sum rate with respect to the duplex mode of the t-th iteration $\boldsymbol{\lambda}^{(t)}$, respectively. These rates are calculated by the hybrid BF designed by Algorithm 1 and 2 corresponding to $\boldsymbol{\lambda}^{(t)}$. The proposed duplex mode selection algorithm can be divided into two main steps:

1) Switching step: At each iteration t, we find the worst SBS with the lowest end-to-end data rate among all SBSs as

$$l^{(t)} = \arg\min_{l} R_l(\boldsymbol{\lambda}^{(t)}) \tag{46}$$

Then, we switch the duplex mode of the $l^{(t)}$-th SBS and update $\boldsymbol{\lambda}^{(t)}$ as $\boldsymbol{\lambda}^{(t+1)}$. Next, we compute the system sum rate $R^{\mathsf{sum}}(\boldsymbol{\lambda}^{(t+1)})$ and compare it with $R^{\mathsf{sum}}(\boldsymbol{\lambda}^{(t)})$. If $R^{\mathsf{sum}}(\boldsymbol{\lambda}^{(t+1)}) > R^{\mathsf{sum}}(\boldsymbol{\lambda}^{(t)})$, we repeat the switching step and stop the switching step, otherwise.

2) Exploration step: To explore new cases for improving the system sum rate, we introduce the exploration step. During each exploration iteration m, if $R^{\mathsf{sum}}(\boldsymbol{\lambda}^{(t+1)}) < R^{\mathsf{sum}}(\boldsymbol{\lambda}^{(t)})$, we select the SBS index as $l_{\mathsf{ex}}^{(m)} = \mathrm{mod}(m-1, L)+1$ and switch the duplex mode of the $l_{\mathsf{ex}}^{(m)}$-th SBS in $\boldsymbol{\lambda}^{(t)}$ to obtain the new candidate duplex mode $\boldsymbol{\lambda}_{\mathsf{ex}}^{(t+1)}$. Then, $\boldsymbol{\lambda}_{\mathsf{ex}}^{(t+1)}$ will be used as the initial duplex mode vector at the next switching step if $R^{\mathsf{sum}}(\boldsymbol{\lambda}_{\mathsf{ex}}^{(t+1)}) > R^{\mathsf{sum}}(\boldsymbol{\lambda}^{(t)})$. On the other hand, if $R^{\mathsf{sum}}(\boldsymbol{\lambda}_{\mathsf{ex}}^{(t+1)}) < R^{\mathsf{sum}}(\boldsymbol{\lambda}^{(t)})$, the exploration step is repeated. The algorithm stops when there is no sum rate improvement for L consecutive exploration iterations.

The proposed WMS mode selection algorithm is summarized in Algorithm 3. From the proposed algorithms, we can obtain sub-optimal duplex mode $\boldsymbol{\lambda}^{\star}$ and the hybrid BF corresponding to $\boldsymbol{\lambda}^{\star}$ which is optimized at the Step 6 or 10 in Algorithm 3. It can be confirmed that the sum rate does not decrease over iterations, thus the WMS algorithm converges to a local optimum point due to the limited transmit power of the BSs, which imposes an upper bounded sum rate. We note that although the WMS algorithm is similar to branch-and-bound algorithm, there are distinct differences between them. Branch-and-bound is well-known technique to obtain optimal solutions in integer programming. It explores all possible solutions through tree traversal using bounds to prune branches, but exhibits worst-case exponential time complexity. Unlike the BB method, the proposed WMS selectively explores the neighborhood of the current solution by modifying only the duplex

Authorized licensed use limited to: Univ Of Incheon. Downloaded on October 26,2026 at 13:17:40 UTC from IEEE Xplore. Restrictions apply.

Algorithm 3 Worst Mode Switching (WMS) Algorithm

Set the iteration count $t = 1$ and $m = 1$
Initialize $\boldsymbol{\lambda}^{(1)}$ as an arbitrary duplex mode vector and calculate $R^{\mathsf{sum}}(\boldsymbol{\lambda}^{(t)})$ through Algorithm 1 and 2
repeat
  Find the SBS cell with the lowest end-to-end data rate $l^{(t)} = \arg\min_l R_l(\boldsymbol{\lambda}^{(t)})$
  Switch the duplex mode of the $l^{(t)}$th SBS and update $\boldsymbol{\lambda}^{(t)}$ as $\boldsymbol{\lambda}^{(t+1)}$
  Calculate $R^{\mathsf{sum}}(\boldsymbol{\lambda}^{(t+1)})$ through Algorithm 1 and 2
  while $R^{\mathsf{sum}}(\boldsymbol{\lambda}^{(t+1)}) < R^{\mathsf{sum}}(\boldsymbol{\lambda}^{(t)})$ **do**
    $l_{\mathsf{ex}}^{(m)} \leftarrow \mathrm{mod}(m-1, L) + 1$
    Switch the duplex mode of the $l_{\mathsf{ex}}^{(m)}$th SBS in $\boldsymbol{\lambda}^{(t)}$ to obtain $\boldsymbol{\lambda}_{\mathsf{ex}}^{(t+1)}$
    Calculate $R^{\mathsf{sum}}(\boldsymbol{\lambda}_{\mathsf{ex}}^{(t+1)})$ through Algorithm 1 and 2
    if $R^{\mathsf{sum}}(\boldsymbol{\lambda}_{\mathsf{ex}}^{(t+1)}) > R^{\mathsf{sum}}(\boldsymbol{\lambda}^{(t)})$ **then**
      $\boldsymbol{\lambda}^{(t+1)} \leftarrow \boldsymbol{\lambda}_{\mathsf{ex}}^{(t+1)}$
    else
      $m \leftarrow m + 1$
    end if
  end while
  Stopping criterion: Break if there is no change in $\boldsymbol{\lambda}$ after L consecutive exploration iterations
  $t \leftarrow t + 1$
until Stopping criterion is achieved
return: $\boldsymbol{\lambda}^{\star}, \mathbf{F}^{\mathsf{BB}}, \mathbf{W}_l^{\mathsf{RF}}, \mathbf{W}_l^{\mathsf{BB}}, \forall l \in \mathcal{L}$

mode of SBS with the worst rate, which is the switching step. Thus, WMS does not maintain or explore a solution tree structure, resulting in polynomial time complexity. In short, WMS is a heuristic algorithm searching in the local space and maintaining a polynomial complexity, whereas BB searches the global space and has exponential complexity. We will show through simulation, however, that the performance of WMS achieves closely to an exhaustive search.

B. Scenario With Statistical and Imperfect CSI

To implement the proposed algorithm, MBS and SBSs should share perfect instantaneous CSI, which may lead to an increase in signaling overhead. Given that the inter-BS channel remains static over a long term period, the CSI of the inter-BS channel can be estimated once within the time interval illustrated in Fig. 2, which reduces signaling overhead for exchanging CSIs. On the other hand, since the CSI of the SBS-UE channel exhibits time-varying characteristics, it is estimated at each frame within the second phase depicted in Fig. 2. Then, each SBS sends the estimated instantaneous CSIs including CTI from MBS and ICI from other SBSs to MBS for operating the proposed algorithm, causing a significant overhead. Instead of collecting instantaneous CSIs of all links at MBS, a signaling overhead can be further reduced by sharing the statistical CSIs of CTI and ICI terms. Moreover, the mobility of UEs makes it challenging to achieve perfect estimation of the CSI of the SBS-UE channel, and therefore it can be more reasonable to assume imperfect CSI in practical systems.

In this subsection, we discuss the implementation of the proposed algorithm with imperfect and statistical CSIs. Due to channel estimation error, the l-th SBS obtain the imperfect CSI as $\hat{\mathbf{g}}_{l,l,k} = \tilde{\mathbf{g}}_{l,l,k} - \mathbf{e}_{l,l,k}$ where $\mathbf{e}_{l,l,k}$ is the estimation error with Gaussian distribution and $\tilde{\mathbf{g}}_{j,l,k} = \mathbf{g}_{j,l,k}\mathbf{W}^{\mathsf{RF}}$ is the effective channel from the j-th SBS to the k-th UE served by the l-th SBS. Since we have the imperfect CSI and the statistical information of CTI and ICI terms not instantaneous information, a lower bound of the first term of $R_{l,k}^{\mathsf{A}}$ in (47) is derived as shown at the bottom of the page, where $\tilde{\mathsf{IUI}}_{l,k} = \sum_{m\neq k}^{K}(|\hat{\mathbf{g}}_{l,l,k}\mathbf{w}_{l,m}^{\mathsf{BB}}|^2 + |\mathbf{w}_{l,k}^{\mathsf{BB}\mathsf{H}}\boldsymbol{\Phi}_{l,l,k}\mathbf{w}_{l,k}^{\mathsf{BB}}|^2)$, $\mathsf{CTI}_{l,k} = \sum_{j=1}^{L}\frac{P_{\mathsf{B}}}{P_{\mathsf{A}}}|\tilde{\mathbf{g}}_{0,l,k}\mathbf{f}_j^{\mathsf{BB}}|^2$, $\mathsf{ICI}_{j,l,k} = |\tilde{\mathbf{g}}_{j,l,k}\mathbf{w}_{j,m}^{\mathsf{BB}}|^2$, and $\tilde{\sigma}^2 = P_{\mathsf{A}} \cdot \left(\mathbb{E}[\mathsf{CTI}_{l,k}] + \sum_{j\neq l}^{L}\mathbb{E}[\mathsf{ICI}_{j,l,k}]\right) + \sigma^2$.

In a similar manner, the lower bound of the second term of $\gamma_{l,k}^{\mathsf{A}}$ in (47) can be obtained. Since these lower bounds can be transformed into Rayleigh quotient form as in Section iv.B, the proposed algorithm, i.e., GPI-based BB BF optimization algorithm and WMS algorithm, can be easily applied even in the case of imperfect and statistical CSI [43], [45].

C. Complexity Analysis

In Algorithm 1, the main computational load is introduced from the construction of $\mathbf{R}_l^z$ in Step 9 whose complexity is $\mathcal{O}(KN^t|\mathcal{W}_{l,\mathsf{lb}}^z|)$ and the max operation in Step 11 whose complexity is $\mathcal{O}(KN^t\log(KN^t))$. Since these steps are repeated over K times for L SBSs, the computational complexity of the Alg. 1 is $\mathcal{O}(LK^2N^{\mathsf{t}}(|\mathcal{W}_{l,\mathsf{lb}}^z| + \log(KN^t)))$. In Algorithm 2, the major computational load is calculating the inversion of $\mathbf{Y}_{\mathsf{KKT}}$. Since $\mathbf{Y}_{\mathsf{KKT}}$ is a block diagonal matrix comprised of one $L\times L$ sub-block symmetric matrix and L $K\times K$ sub-block symmetric matrices, the inversion of $\mathbf{Y}_{\mathsf{KKT}}$ can be obtained by calculating the inversion of each sub-matrix. Therefore, the complexity of Algorithm 2 is $\mathcal{O}\left(\frac{1}{3}I_2(L^3 + LK^3)\right)$, where I_2 is the number of the iteration. For Algorithm 3, the main computational load is the max operation in Step 4 whose complexity is $\mathcal{O}(L\log(L))$. Therefore, the overall complexity is in the order of $\mathcal{O}(I_3L\log(L)(LK^2N^{\mathsf{t}}(|\mathcal{W}_{l,\mathsf{lb}}^z| + \log(KN^t))+$

$$\log_2(1+\gamma_{l,k}^{\mathsf{A},1}) \geq \log_2\left(1 + \frac{\lambda_l\left|\hat{\mathbf{g}}_{l,l,k}\mathbf{w}_{l,k}^{\mathsf{BB}}\right|^2}{\lambda_l\left|\mathbf{w}_{l,k}^{\mathsf{BB}\mathsf{H}}\mathbb{E}[\mathbf{e}_{l,l,k}^{\mathsf{H}}\mathbf{e}_{l,l,k}]\mathbf{w}_{l,k}^{\mathsf{BB}}\right|^2 + \lambda_l\tilde{\mathsf{IUI}}_{l,k} + \mathbb{E}[\mathsf{CTI}_{l,k}] + \sum_{j\neq l}^{L}\mathbb{E}[\mathsf{ICI}_{j,l,k}] + \frac{\sigma^2}{P_{\mathsf{A}}}}\right)$$
$$= \log_2\left(1 + \frac{\lambda_l\left|\hat{\mathbf{g}}_{l,l,k}\mathbf{w}_{l,k}^{\mathsf{BB}}\right|^2}{\lambda_l\left|\mathbf{w}_k^{\mathsf{BB}\mathsf{H}}\boldsymbol{\Phi}_{l,l,k}\mathbf{w}_k^{\mathsf{BB}}\right|^2 + \lambda_l\tilde{\mathsf{IUI}}_{l,k} + \frac{\tilde{\sigma}^2}{P_{\mathsf{A}}}}\right) = \hat{R}_{l,k}^{\mathsf{A},1} \tag{47}$$

Authorized licensed use limited to: Univ Of Incheon. Downloaded on October 26,2026 at 13:17:40 UTC from IEEE Xplore. Restrictions apply.

TABLE I
SYSTEM PARAMETERS

Notation	Parameter	Value
L	Number of SBSs	6
K	Number of UEs in each SBS cell	3
N^{d}	Number of antenna with MBS	64
N^{t}	Number of transmit antennas of each SBS	36
N^{r}	Number of receive antennas of each SBS	36
P_{B}	Maximum transmit power of MBS	46dBm
P_{A}	Maximum transmit power of SBS	30dBm
W	System bandwidth	200MHz
f_c	Carrier frequency	28GHz
N_0	Noise variance	-174dBm/Hz
σ^2_{SI}	SIC error variance	-100dB
B	Number of ADC bit	11
$\delta_l/\delta_{l,k}$	Maximum tolerance level of inter-SBS/inter-cell interference	-110dB

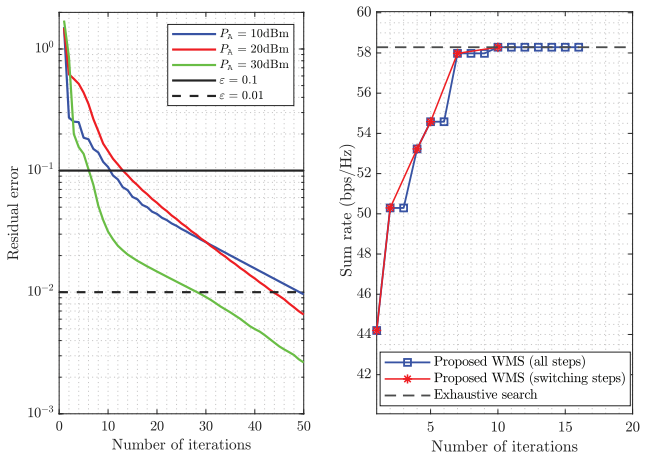
$\frac{1}{3}I_2(L^3+LK^3)))$ where I_3 is the required number of iterations for Algorithm 3.

VI. PERFORMANCE EVALUATION

In this section, we evaluate the proposed algorithms through various simulations by comparing our algorithms with several benchmark schemes and analyzing the impact of system parameters on performance. We consider a cell with a radius of 250m, where MBS is located at the center, and 6 SBSs are deployed in fixed locations. The l-th SBS is located at $[180(\cos(2\pi l/6))\text{m}, 180(\sin(2\pi l/6))\text{m}]$ at an example. Also, 3 UEs are randomly deployed in each SBS cell with a radius of 40m, and there are 18 UEs in the network. For Algorithm 2, we set $\epsilon = 0.01$ and $\alpha_{l,0} = 0.5$; if Algorithm 2 does not converge after 50 iterations, we adjust the parameter α_l as $\alpha_{l,n+1} = \alpha_{l,n} + 0.5$. Unless specifically specified, we use the system parameters in Table I.

For comparison, we use the following benchmark schemes:

- **Full-duplex (FD)**: All the SBSs operate in full-duplex mode. If a SBS does not satisfy the constraints (21) and (26b), then it operates in half-duplex mode.
- **Half-duplex (HD)**: All the SBSs operate in half-duplex mode.
- **Random mode selection (RMS)**: Each SBS randomly selects its duplex mode. If an FD SBS does not satisfy the constraints (21) and (26b), it operates in half-duplex mode.
- **Sequential mode selection (SMS)**: By fixing the duplex mode at other SBSs, each SBS finds the RF beams for both full-duplex and half-duplex using Algorithm 1, and then determines the duplex mode and RF beams with a higher value for (24). This process is performed sequentially until the objective function (24) converges.
- **Minimum mean square error (MMSE) precoding**: The MMSE precoding is utilized for BB BF of MBS and SBSs by only considering IBI and IUI, respectively.
- **Zero-forcing (ZF) precoding**: The ZF precoding and the water-filling power allocation are utilized for BB BF of MBS and SBSs by only considering IBI and IUI, respectively.



(a) Convergence of Alg. 2 (b) Convergence of Alg. 3

Fig. 3. Convergence behavior of the proposed algorithms.

- **Maximum ratio combining (MRT) precoding**: The MRT precoding is utilized for BB BF of MBS and SBSs.
- **Channel power based greedy beam selection (CP)**: The greedy beam selection with only beam domain channel power is adopted as in Algorithm 1, and it is performed while disregarding constraint (26b) and setting $f_{l,k}(x) = x$ in (28) for only considering the channel gain.

As an abbreviation rule, we denote **B-R** as a hybrid BF benchmark scheme, where **R** is used for RF BF design, and **B** is used for BB BF design.

A. Convergence Behavior of the Proposed Algorithms

In Fig. 3, we present the convergence behaviors of Algorithm 2 and Algorithm 3. Fig. 3(a) presents the residual error $\|\mathbf{q}^{(t)} - \mathbf{q}^{(t-1)}\|$ over the number of iterations. As shown in Fig. 3(a), Algorithm 2 converges within 50 iterations, indicating that we can find the best local optimal point by using the proposed GPI algorithm. In Fig. 3(b), we compare the system sum rate performance of Algorithm 3 with an exhaustive duplex mode search. The proposed WMS algorithm converges exactly to exhaustive search within 10 iterations, demonstrating that the algorithm can find an optimal or a near-optimal solution with low complexity.

B. Performance Evaluation of Hybrid-Duplex Wireless Backhaul Network

Fig. 4 presents the percentage of SBSs operating in FD mode versus the number of ADC bits with different number of antennas at the SBS. As the number of ADC bits decreases, we can observe that the ratio of SBSs operating in FD mode decreases. A smaller number of ADC bits leads to a lower η_{ADC} value in (20), which limits the possible beam combinations for satisfying the ADC saturation constraint in (19). With fewer FD beam combinations, it is difficult to enhance the channel gain of associated UEs while suppressing the inter-cell and inter-SBS interference. Consequently, selecting the HD mode at each SBS is more preferable if the number of ADC bits is small since HD mode can utilize all beam combinations

Authorized licensed use limited to: Univ Of Incheon. Downloaded on October 26,2026 at 13:17:40 UTC from IEEE Xplore. Restrictions apply.

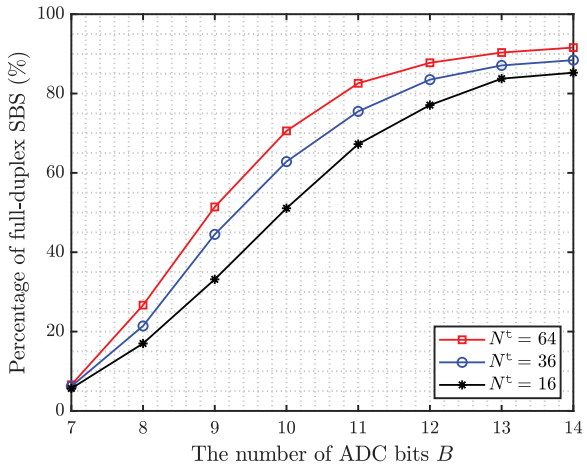


Fig. 4. The percentage of full-duplex SBSs versus the number of ADC bits B.

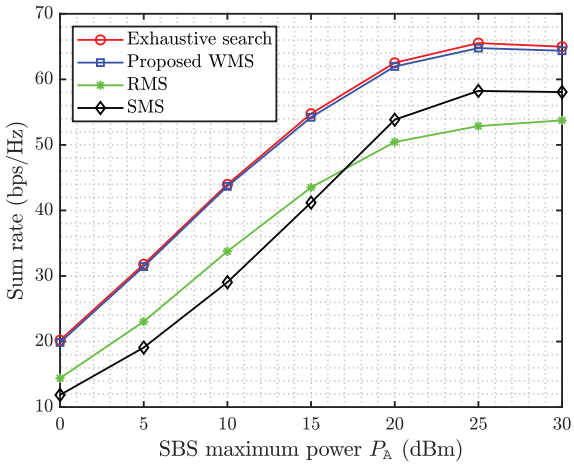


Fig. 6. Comparison of different duplex mode selection schemes.

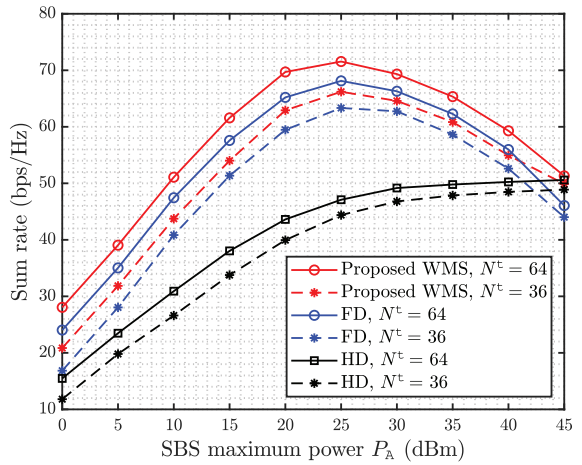


Fig. 5. Sum rate versus the SBS maximum transmit power P_{A} for comparison of different duplex mode selections with $N^{\mathrm{t}} = 64$ and $N^{\mathrm{t}} = 36$.

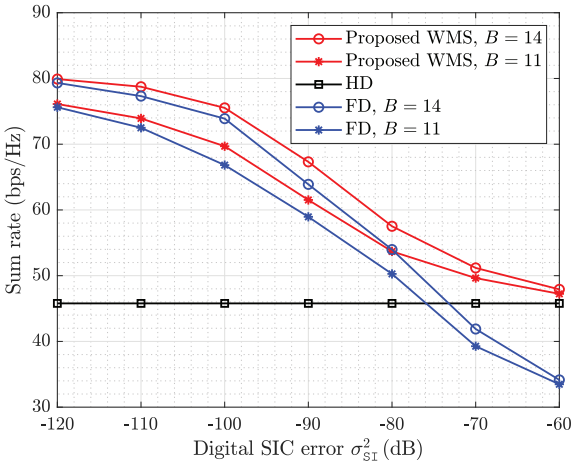


Fig. 7. The effect of digital SIC error σ^2_{SI} on sum rate with different numbers of ADC bits.

from a codebook. On the other hand, as the number of ADC bits increases, more FD beam combinations are available, which can effectively mitigate additional interference arising from SBSs operating in FD mode. Furthermore, it can be observed from Fig. 4 shows that the ratio of SBSs operating in FD mode increases as the number of antennas at SBS increases, since the number of possible beams satisfying the ADC saturation constraint increases. The increase in ratio of FD SBSs however reaches a saturation, suggesting that there is an optimal range for the number of ADC bits which is around 13 or 14.

Fig. 5 demonstrates the sum rate performance versus the SBS maximum power P_{A} for $N^{\mathrm{t}} = 64$ and $N^{\mathrm{t}} = 36$. When all SBSs operate in FD mode, the sum rate initially increases and then decreases as P_{A} increases, eventually leading to a lower sum rate than HD mode. This phenomenon is caused by the limited beam combinations of FD mode satisfying the ADC saturation constraint. Specifically, in the interference-limited region with relatively high P_{A}, the available beam combinations for satisfying the ADC saturation are significantly reduced, causing limited DoF for mitigating ISI and ICI, and resulting in a decrease in the sum rate. On the other hand, since the proposed WMS algorithm adaptively selects the duplex mode by accounting for the possible beam combinations, it always provides a better sum rate performance than other schemes. At high P_{A}, the proposed WMS achieves similar performance to HD mode because there are a few beam combinations satisfying the ADC saturation constraint, and thus the proposed algorithm tends to select HD mode with high P_{A}.

Fig. 6 demonstrates the effects of the proposed WMS algorithm for duplex mode selection. The WMS algorithm outperforms both RMS and SMS schemes. The performance of SMS is worse than that of the WMS algorithm, since it does not jointly consider mode selection and hybrid BF. Furthermore, it can be observed that the performance of WMS algorithm closely approaches to that of an exhaustive search while having much lower complexity. This result demonstrates the near-optimality of the proposed WMS algorithm.

Fig. 7 demonstrates the system sum rate performance versus the amount of digital SIC error σ^2_{SI} when the ADC resolution is 14 bits and 11 bits. When all SBSs operate in FD mode, the sum rate decreases as the SIC error increases, reaching a

Authorized licensed use limited to: Univ Of Incheon. Downloaded on October 26,2026 at 13:17:40 UTC from IEEE Xplore. Restrictions apply.

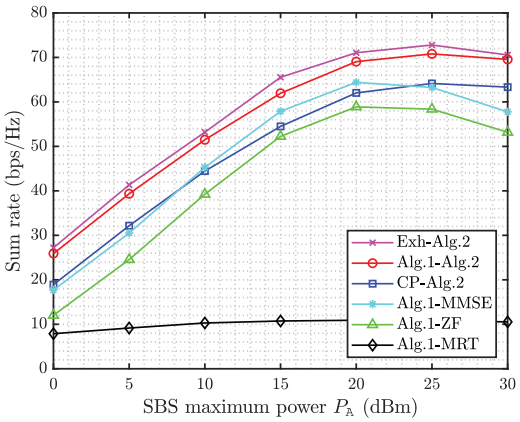


Fig. 8. Comparison of different hybrid BF schemes with respect to SBS maximum transmit power P_{A}.

lower value compared to when all SBSs operate in HD mode, a similar phenomenon as also observed in Fig. 5. This sum rate degradation is due to the increased power of residual self-interference after digital SIC as in (10), leading to a decrease of backhaul data rate and end-to-end data rate at FD SBS cells in (17) and (18). On the other hand, our proposed WMS algorithm outperforms both FD and HD mode selections for 14 bits and 11 bits of ADC resolution, since it flexibly selects the duplex mode depending on the amount of digital SIC error. Specifically, in the WMS algorithm, all the SBSs tend to select FD mode when σ_{SI}^2 is small, and conversely, select HD mode when σ_{SI}^2 is high. The results in Fig. 5 and Fig. 7 demonstrate the effectiveness of the proposed WMS algorithm to adaptively select the duplex mode depending on system parameters such as the SBS maximum transmit power, ADC resolution bits and the amount of digital SIC errors.

Fig. 8 demonstrates the effects of the proposed algorithms for hybrid BF design. In Fig. 8, bfExh in **Exh-** Alg. 2 represents the exhaustive search used to find the best RF beam selection. It can be confirmed that the proposed algorithm can achieve performance comparable to the exhaustive search method with lower complexity. Also, we can observe that the proposed algorithm exhibits better performance compared to other benchmark schemes. CP performs worse than Algorithm 1, since it selects RF beams to maximize the channel gain of the access link without considering ISI and ICI. Moreover, we can observe that the proposed GPI algorithm outperforms MMSE and ZF because MMSE and ZF can eliminate only IBI and IUI, while the proposed GPI algorithm suppresses all interferences (IBI, IUI, ISI, ICI, CTI, and residual SI) in a multi-cell wireless backhaul network.

VII. Conclusion

In this paper, we proposed the optimization framework for hybrid BF design and duplex mode selection in mmWave multi-cell wireless backhaul networks where each SBS can dynamically select its duplex mode. For the hybrid BF design, we presented our two-stage approach where the first stage employs a greedy RF and the second uses a GPI based BB BF optimization algorithm. Then, we provided the WMS algorithm for duplex mode selection which switches the mode of SBS having the worst rate and provides a near-optimal solution in polynomial time. Simulation results showed that the proposed algorithm adapts well to the system parameters including the number of ADC bits and residual SIC, and provides a higher system sum rate compared to all benchmark schemes.

Appendix

The Lagrangian function corresponding to the problem (41) is defined as

$$L_1(\mathbf{q}) = \sum_{l=1}^{L} -\alpha_l \ln\Big(m_l(\mathbf{q}) + n_l(\mathbf{q})\Big). \tag{48}$$

A stationary point that satisfies the first-order KKT condition can be obtained by taking the partial derivative of $L_1(\mathbf{q})$ with respect to $\mathbf{q}$ and setting to zero. This can be represented as

$$\frac{\partial L_1(\mathbf{q})}{\partial \mathbf{q}^{\mathsf{H}}} = \sum_{l=1}^{L} -u_l(\mathbf{q})\left(\frac{\partial m_l(\mathbf{q})}{\partial \mathbf{q}^{\mathsf{H}}} + \frac{\partial n_l(\mathbf{q})}{\partial \mathbf{q}^{\mathsf{H}}}\right) = 0. \tag{49}$$

The partial derivative of $m_l(\mathbf{q})$ and $n_l(\mathbf{q})$ can be obtained as

$$\frac{\partial m_l(\mathbf{q})}{\partial \mathbf{q}^{\mathsf{H}}} = \beta_l m_l(\mathbf{q})\left(\left(\frac{\mathbf{A}_l^1\mathbf{q}}{\mathbf{q}^{\mathsf{H}}\mathbf{A}_l^1\mathbf{q}} - \frac{\mathbf{B}_l^1\mathbf{q}}{\mathbf{q}^{\mathsf{H}}\mathbf{B}_l^1\mathbf{q}}\right) + \left(\frac{\mathbf{A}_l^2\mathbf{q}}{\mathbf{q}^{\mathsf{H}}\mathbf{A}_l^2\mathbf{q}} - \frac{\mathbf{B}_l^2\mathbf{q}}{\mathbf{q}^{\mathsf{H}}\mathbf{B}_l^2\mathbf{q}}\right)\right). \tag{50}$$

$$\frac{\partial n_l(\mathbf{q})}{\partial \mathbf{q}^{\mathsf{H}}} = \sum_{k=1}^{K}\beta_l n_l(\mathbf{q})\left(\left(\frac{\mathbf{C}_{l,k}^1\mathbf{q}}{\mathbf{q}^{\mathsf{H}}\mathbf{C}_{l,k}^1\mathbf{q}} - \frac{\mathbf{D}_{l,k}^1\mathbf{q}}{\mathbf{q}^{\mathsf{H}}\mathbf{D}_{l,k}^1\mathbf{q}}\right) + \left(\frac{\mathbf{C}_{l,k}^2\mathbf{q}}{\mathbf{q}^{\mathsf{H}}\mathbf{C}_{l,k}^2\mathbf{q}} - \frac{\mathbf{D}_{l,k}^2\mathbf{q}}{\mathbf{q}^{\mathsf{H}}\mathbf{D}_{l,k}^2\mathbf{q}}\right)\right). \tag{51}$$

Then, by substituting (50) and (51) into (49), we can obtain the following first-order KKT condition

$$\begin{aligned}&\sum_{l=1}^{L}\beta_l u_l(\mathbf{q})\left(m_l(\mathbf{q})\left(\frac{\mathbf{A}_l^1}{\mathbf{q}^{\mathsf{H}}\mathbf{A}_l^1\mathbf{q}} + \frac{\mathbf{A}_l^2}{\mathbf{q}^{\mathsf{H}}\mathbf{A}_l^1\mathbf{q}}\right) + n_l(\mathbf{q})\sum_{k=1}^{K}\left(\frac{\mathbf{C}_{l,k}^1}{\mathbf{q}^{\mathsf{H}}\mathbf{C}_{l,k}^1\mathbf{q}} + \frac{\mathbf{C}_{l,k}^2}{\mathbf{q}^{\mathsf{H}}\mathbf{C}_{l,k}^2\mathbf{q}}\right)\right)\mathbf{q}\\ &= \sum_{l=1}^{I}\beta_l u_l(\mathbf{q})\left(m_l(\mathbf{q})\left(\frac{\mathbf{B}_l^1}{\mathbf{q}^{\mathsf{H}}\mathbf{B}_l^1\mathbf{q}} + \frac{\mathbf{B}_l^2}{\mathbf{q}^{\mathsf{H}}\mathbf{B}_l^1\mathbf{q}}\right) + n_l(\mathbf{q})\sum_{k=1}^{K}\left(\frac{\mathbf{D}_{l,k}^1}{\mathbf{q}^{\mathsf{H}}\mathbf{D}_{l,k}^1\mathbf{q}} + \frac{\mathbf{D}_{l,k}^2}{\mathbf{q}^{\mathsf{H}}\mathbf{D}_{l,k}^2\mathbf{q}}\right)\right)\mathbf{q}\end{aligned} \tag{52}$$

This first-order KKT condition can be represented as in Lemma 1.□

References

[1] R. W. Heath, N. González-Prelcic, S. Rangan, W. Roh, and A. M. Sayeed, "An overview of signal processing techniques for millimeter wave MIMO systems," *IEEE J. Sel. Topics Signal Process.*, vol. 10, no. 3, pp. 436–453, Apr. 2016.

[2] NR; Study on Integrated Access and Backhaul, Standard TR 38.874 (Rel. 16), TR 38.874 (Rel. 16), Dec. 2018.

Authorized licensed use limited to: Univ Of Incheon. Downloaded on October 26,2026 at 13:17:40 UTC from IEEE Xplore. Restrictions apply.

[3] G. Kwon and H. Park, "Joint user association and beamforming design for millimeter wave UDN with wireless backhaul," *IEEE J. Sel. Areas Commun.*, vol. 37, no. 12, pp. 2653–2668, Dec. 2019.

[4] L. F. Abanto-Leon, A. Asadi, A. Garcia-Saavedra, G. H. Sim, and M. Hollick, "RadiOrchestra: Proactive management of millimeter-wave self-backhauled small cells via joint optimization of beamforming, user association, rate selection, and admission control," *IEEE Trans. Wireless Commun.*, vol. 22, no. 1, pp. 153–173, Jan. 2023.

[5] C. Saha and H. S. Dhillon, "Millimeter wave integrated access and backhaul in 5G: Performance analysis and design insights," *IEEE J. Sel. Areas Commun.*, vol. 37, no. 12, pp. 2669–2684, Dec. 2019.

[6] J.-H. Kwon, B. Lim, and Y.-C. Ko, "Resource allocation and system design of out-band based integrated access and backhaul network at mmWave band," *IEEE Trans. Veh. Technol.*, vol. 71, no. 6, pp. 6503–6517, Jun. 2022.

[7] B. Lim et al., "Joint association and resource allocation for multi-hop integrated access and backhaul (IAB) network," *J. Commun. Netw.*, vol. 25, no. 4, pp. 440–455, Aug. 2023.

[8] M. Mohammadi, Z. Mobini, D. Galappaththige, and C. Tellambura, "A comprehensive survey on full-duplex communication: Current solutions, future trends, and open issues," *IEEE Commun. Surveys Tuts.*, vol. 25, no. 4, pp. 2190–2244, 4th Quart., 2023.

[9] *New SID on Smart Repeaters for NR*, document RP-201139, Jun. 2020.

[10] G. Y. Suk, S.-M. Kim, J. Kwak, S. Hur, E. Kim, and C.-B. Chae, "Full duplex integrated access and backhaul for 5G NR: Analyses and prototype measurements," *IEEE Wireless Commun.*, vol. 29, no. 4, pp. 40–46, Aug. 2022.

[11] E. Everett, A. Sahai, and A. Sabharwal, "Passive self-interference suppression for full-duplex infrastructure nodes," *IEEE Trans. Wireless Commun.*, vol. 13, no. 2, pp. 680–694, Feb. 2014.

[12] J. W. Kwak, M. S. Sim, I.-W. Kang, J. Park, K.-K. Wong, and C.-B. Chae, "Analog self-interference cancellation With practical RF components for full-duplex radios," *IEEE Trans. Wireless Commun.*, vol. 22, no. 7, pp. 4552–4564, Jul. 2023.

[13] J. Kim et al., "On the learning of digital self-interference cancellation in full-duplex radios," *IEEE Wireless Commun.*, vol. 31, no. 4, pp. 184–191, Aug. 2024.

[14] I. P. Roberts, J. G. Andrews, H. B. Jain, and S. Vishwanath, "Millimeter-wave full duplex radios: New challenges and techniques," *IEEE Wireless Commun.*, vol. 28, no. 1, pp. 36–43, Feb. 2021.

[15] Y. Zhang, M. Xiao, S. Han, M. Skoglund, and W. Meng, "On precoding and energy efficiency of full-duplex millimeter-wave relays," *IEEE Trans. Wireless Commun.*, vol. 18, no. 3, pp. 1943–1956, Mar. 2019.

[16] I. P. Roberts and S. Vishwanath, "Beamforming cancellation design for millimeter-wave full-duplex," in *Proc. IEEE Global Commun. Conf. (GLOBECOM)*, Dec. 2019, pp. 1–6.

[17] L. Zhu, J. Zhang, Z. Xiao, X. Cao, X. Xia, and R. Schober, "Millimeter-wave full-duplex UAV relay: Joint positioning, beamforming, and power control," *IEEE J. Sel. Areas Commun.*, vol. 38, no. 9, pp. 2057–2073, Sep. 2020.

[18] I. P. Roberts, J. G. Andrews, and S. Vishwanath, "Hybrid beamforming for millimeter wave full-duplex under limited receive dynamic range," *IEEE Trans. Wireless Commun.*, vol. 20, no. 12, pp. 7758–7772, Dec. 2021.

[19] G. Y. Suk, J. Kwak, J. Choi, and C.-B. Chae, "Dynamic RF beam codebook reduction for cost-efficient mmWave full-duplex systems," in *Proc. GLOBECOM IEEE Global Commun. Conf.*, Dec. 2022, pp. 3809–3814.

[20] I. P. Roberts, A. Chopra, T. Novlan, S. Vishwanath, and J. G. Andrews, "Steer: Beam selection for full-duplex millimeter wave communication systems," *IEEE Trans. Commun.*, vol. 70, no. 10, pp. 6902–6917, Oct. 2022.

[21] E. Chen, M. Tao, and N. Zhang, "User-centric joint access-backhaul design for full-duplex self-backhauled wireless networks," *IEEE Trans. Commun.*, vol. 67, no. 11, pp. 7980–7993, Nov. 2019.

[22] Y. Li, P. Fan, L. Liu, and Y. Yi, "Distributed MIMO precoding for in-band full-duplex wireless backhaul in heterogeneous networks," *IEEE Trans. Veh. Technol.*, vol. 67, no. 3, pp. 2064–2076, Mar. 2018.

[23] N. Forouzan, A. M. Rabiei, M. Vehkaperä, and R. Wichman, "A distributed resource allocation scheme for self-backhauled full-duplex small cell networks," *IEEE Trans. Veh. Technol.*, vol. 70, no. 2, pp. 1461–1473, Feb. 2021}.

[24] M. Mohammadi, T. T. Vu, H. Q. Ngo, and M. Matthaiou, "Network-assisted full-duplex cell-free massive MIMO: Spectral and energy efficiencies," *IEEE J. Sel. Areas Commun.*, vol. 41, no. 9, pp. 2833–2851, Sep. 2023.

[25] A. Chowdhury and C. R. Murthy, "Half-duplex APs with dynamic TDD versus full-duplex APs in cell-free systems," *IEEE Trans. Commun.*, vol. 72, no. 7, pp. 3856–3872, Jul. 2024.

[26] J. Lee and T. Q. S. Quek, "Hybrid full-/half-duplex system analysis in heterogeneous wireless networks," *IEEE Trans. Wireless Commun.*, vol. 14, no. 5, pp. 2883–2895, May 2015.

[27] S. Akbar, Y. Deng, A. Nallanathan, M. Elkashlan, and G. K. Karagiannidis, "Massive multiuser MIMO in heterogeneous cellular networks with full duplex small cells," *IEEE Trans. Wireless Commun.*, vol. 65, no. 11, pp. 4704–4719, Nov. 2017.

[28] Z. Sattar, J. V. D. C. Evangelista, G. Kaddoum, and N. Batani, "Full-duplex two-tier heterogeneous network with decoupled access: Cell association, coverage, and spectral efficiency analysis," *IEEE Access*, vol. 8, pp. 172982–172995, 2020.

[29] S. Haghgoy, M. Mohammadi, Z. Mobini, and K.-K. Wong, "Decoupled UL/DL user association in wireless-powered HetNets with full-duplex small cells," *IEEE Trans. Veh. Technol.*, vol. 72, no. 11, pp. 14341–14355, Nov. 2023.

[30] D. Wang, C. Huang, H. Zhang, S. Jiang, G. Shi, and T. Li, "Dynamic clustering and resource allocation using deep reinforcement learning for smart-duplex networks," *IEEE Internet Things J.*, vol. 10, no. 1, pp. 42–56, Jan. 2023.

[31] T. Riihonen, S. Werner, and R. Wichman, "Hybrid full-duplex/half-duplex relaying with transmit power adaptation," *IEEE Trans. Wireless Commun.*, vol. 10, no. 9, pp. 3074–3085, Sep. 2011.

[32] I. P. Roberts, A. Chopra, T. Novlan, S. Vishwanath, and J. G. Andrews, "Spatial and statistical modeling of multi-panel millimeter wave self-interference," *IEEE J. Sel. Areas Commun.*, vol. 41, no. 9, pp. 2780–2795, Sep. 2023.

[33] B. Yu et al., "Realizing high power full duplex in millimeter wave system: Design, prototype and results," *IEEE J. Sel. Areas Commun.*, vol. 41, no. 9, pp. 2893–2906, Sep. 2023.

[34] S. Hur, T. Kim, D. J. Love, J. V. Krogmeier, T. A. Thomas, and A. Ghosh, "Millimeter wave beamforming for wireless backhaul and access in small cell networks," *IEEE Trans. Commun.*, vol. 61, no. 10, pp. 4391–4403, Oct. 2013.

[35] A. Alkhateeb, O. El Ayach, G. Leus, and R. W. Heath, "Channel estimation and hybrid precoding for millimeter wave cellular systems," *IEEE J. Sel. Topics Signal Process.*, vol. 8, no. 5, pp. 831–846, Oct. 2014.

[36] *Guidelines For Evaluation of Radio Interface Technologies For IMT-2020*, document M.2412, ITU-R WP 5D, ITU-R, 2017.

[37] Z. Guo, X. Wang, and W. Heng, "Millimeter-wave channel estimation based on 2-D beamspace MUSIC method," *IEEE Trans. Wireless Commun.*, vol. 16, no. 8, pp. 5384–5394, Aug. 2017.

[38] J. Zhang, D. Rakhimov, and M. Haardt, "Gridless channel estimation for hybrid mmWave MIMO systems via tensor-ESPRIT algorithms in DFT beamspace," *IEEE J. Sel. Topics Signal Process.*, vol. 15, no. 3, pp. 816–831, Apr. 2021.

[39] K. Satyanarayana, M. El-Hajjar, P.-H. Kuo, A. Mourad, and L. Hanzo, "Hybrid beamforming design for full-duplex millimeter wave communication," *IEEE Trans. Veh. Technol.*, vol. 68, no. 2, pp. 1394–1404, Feb. 2019.

[40] J. Zhang, H. Luo, N. Garg, A. Bishnu, M. Holm, and T. Ratnarajah, "Design and analysis of wideband in-band-full-duplex FR2-IAB networks," *IEEE Trans. Wireless Commun.*, vol. 21, no. 6, pp. 4183–4196, Jun. 2022.

[41] D. Korpi, T. Riihonen, V. Syrjälä, L. Anttila, M. Valkama, and R. Wichman, "Full-duplex transceiver system calculations: Analysis of ADC and linearity challenges," *IEEE Trans. Wireless Commun.*, vol. 13, no. 7, pp. 3821–3836, Jul. 2014.

[42] C. Shen and H. Li, "On the dual formulation of boosting algorithms," *IEEE Trans. Pattern Anal. Mach. Intell.*, vol. 32, no. 12, pp. 2216–2231, Dec. 2010.

[43] J. Park, J. Choi, N. Lee, W. Shin, and H. V. Poor, "Rate-splitting multiple access for downlink MIMO: A generalized power iteration approach," *IEEE Trans. Wireless Commun.*, vol. 22, no. 3, pp. 1588–1603, Mar. 2023.

[44] A. Alizadeh and M. Vu, "Load balancing user association in millimeter wave MIMO networks," *IEEE Trans. Wireless Commun.*, vol. 18, no. 6, pp. 2932–2945, Jun. 2019.

[45] J. Choi, N. Lee, S.-N. Hong, and G. Caire, "Joint user selection, power allocation, and precoding design with imperfect CSIT for multi-cell MU-MIMO downlink systems," *IEEE Trans. Wireless Commun.*, vol. 19, no. 1, pp. 162–176, Jan. 2020.

Authorized licensed use limited to: Univ Of Incheon. Downloaded on October 26,2026 at 13:17:40 UTC from IEEE Xplore. Restrictions apply.



Seok-Hyun Yoon (Student Member, IEEE) received the B.S. degree in computer and communication engineering and the Ph.D. degree in electrical engineering from Korea University, Seoul, South Korea, in 2017 and 2024, respectively. In 2022, he visited Tufts University, Medford, MA, USA, to conduct collaborative research. His research interests include mmWave/THz beamforming, intelligent reflecting surface (IRS), and full-duplex communication.



Byungju Lim (Member, IEEE) received the B.S. and Ph.D. degrees in electrical engineering from Korea University, Seoul, South Korea, in 2015 and 2021, respectively. In 2021, he was a Research Professor with Korea University. From 2022 to 2023, he was a Post-Doctoral Scholar with the Department of Electrical and Computer Engineering, Tufts University, Medford, MA, USA. Since March 2023, he has been with the Department of Electronic Engineering, Pukyong National University, Busan, South Korea, where he is currently an Assistant Professor. His current research interests include machine learning and signal processing for wireless communication.



Mai Vu (Senior Member, IEEE) received the bachelor's degree in computer systems engineering from the Royal Melbourne Institute of Technology, Melbourne, VIC, Australia, the M.S.E. degree in electrical engineering from the University of Melbourne, Parkville, VIC, Australia, and the Ph.D. degree in electrical engineering from Stanford University, Stanford, CA, USA.

From 2006 to 2008, she was a Lecturer and a Researcher with the School of Engineering and Applied Sciences, Harvard University, MA, USA. From 2009 to 2012, she was an Assistant Professor in electrical and computer engineering with McGill University, QC, Canada. Since 2013, she has been with Tufts University, MA, USA, as an Associate Professor and then a Full Professor in electrical and computer engineering. She conducts research in wireless systems, signal processing, and networked communications. She has published extensively in the areas of millimeter-wave communications, 5G and 6G systems, cooperative and cognitive communications, MIMO wireless, and energy-efficient communications. She has served on the technical program committee for numerous IEEE conferences. She served as a Co-Organizer for the 2017 New England Workshop on Software Defined Radio (NEWSDR'17) at Tufts University and as the Technical Co-Chair for the 2023 IEEE Communication Theory Workshop (CTW), Taiwan. From 2013 to 2016, she was an Editor of IEEE TRANSACTIONS ON WIRELESS COMMUNICATIONS. Since November 2022, she has been an Editor of IEEE TRANSACTIONS ON COMMUNICATIONS.



Young-Chai Ko (Senior Member, IEEE) received the B.Sc. degree in electrical and telecommunication engineering from Hanyang University, Seoul, South Korea, and the M.S.E.E and the Ph.D. degrees in electrical engineering from the University of Minnesota, Minneapolis, MN, USA, in 1999 and 2001, respectively. In 2001, he was with Novatel Wireless as a Research Scientist. In 2001, he joined the Wireless Center, Texas Instruments Inc., San Diego, CA, USA, as a Senior Engineer. He is currently a Professor with the School of Electrical Engineering, Korea University, Seoul, South Korea. His research interests include performance analysis and the design of wireless communication systems.

Authorized licensed use limited to: Univ Of Incheon. Downloaded on October 26,2026 at 13:17:40 UTC from IEEE Xplore. Restrictions apply.